MINISTRY OF AVIATION

AERONAUTICAL RESEARCH COUNCIL
REPORTS AND MEMORANDA

The Characteristics of Some Slender Cambered Gothic Wings at Mach Numbers from 0.4 to 2.0

By L. C. SQUIRE, Ph.D.

The Characteristics of Some Slender Cambered Gothic Wings at Mach Numbers from 0·4 to 2·0

By L. C. Squire, Ph.D.

Communicated by the Deputy Controller Aircraft (Research and Development), Ministry of Aviation

---

Reports and Memoranda No. 3370*
May, 1962

Summary.

Wind-tunnel tests have been made on a series of cambered slender wings of modified gothic planform. The main purpose of these tests was to investigate camber designs which have low lift-dependent drag and a given centre-of-pressure position ahead of the aerodynamic centre.

The results show that at the design conditions the centre-of-pressure position is close to, or slightly ahead of, the design position and the trimming power associated with the forward position of centre of pressure is largely maintained throughout the speed range. The maximum lift/drag ratios of the cambered wings are slightly greater than those of the uncambered wing.

LIST OF CONTENTS

LIST OF TABLES

LIST OF ILLUSTRATIONS

1. *Introduction.*

In the research programme at the Royal Aircraft Establishment on slender wings a principal effort in the 3 ft Tunnel has been concentrated on model shapes designed to check specific features of the theoretical camber-design methods[1, 2, 3]. These shapes have been tested through the whole speed range of the tunnel ($M = 0\cdot4$ to $M = 2\cdot0$), in order to study off-design flow development. Results of tests on the first four wings were reported in Refs. 4 and 5, this report gives results for the next four wings of the series.

Tests[4, 5] on the first series of cambered gothic wings showed that the flow was attached over the whole wing surface for a small incidence range near the design lift coefficient for the full Mach number range of the tests ($0\cdot4$ to $2\cdot0$), and the variation of lift-dependent drag with Mach number was close to that predicted by theory. However, the Mach number range in which the lift-curve

<div align="center">3</div>

slopes and aerodynamic centres (in the attached-flow conditions) were in agreement with slender-wing theory was small. The general trends of these results were, nevertheless, in fair agreement with predictions based on not-so-slender theory, and on linear theory when applied to cropped delta wings[6] approximating to the gothic planform.

The 3 ft Tunnel tests, and tests on similar models in a low-speed tunnel[7], also showed that medium amounts of leading-edge droop increased the amount of non-linear lift compared with that of the uncambered wing, so that at incidences above 10° the cambered wings developed more lift than the plane wing despite their having a positive no-lift angle. However, large droop not only increased the no-lift angle but also decreased the amount of non-linear lift thus leading to a marked loss of lift relative to the uncambered wing. This loss of lift would obviously impair the low-speed characteristics of the configuration.

In the present report, test results are given for a series of cambered* wings with a modified gothic planform (Fig. 1) together with results for the corresponding uncambered wing. The camber surfaces of these models differ from those of the first series in that the centre sections of the present wings have longitudinal camber to move the centre of pressure, at design lift, forward of the aerodynamic centre. It is hoped that camber in this form may provide a low-drag method of trimming out the effect of the rearward shift of aerodynamic centre which takes place between subsonic and supersonic speeds.

2. Details of Models.

Tests were made on four wings† designated by the numbers 5, 6, 7 and 8 (continuing the designation of Refs. 4 and 5). Wing 5 is the basic uncambered wing, while wings 6, 7 and 8 incorporate various amounts of camber, details of which are given below. Geometrical details of the four wings are given in Figs. 1 to 4 and in Table 1; load distributions and velocity distributions associated with the camber design are shown in Figs. 5 to 7.

The camber surfaces of wings 6 and 7 were designed by the method proposed by Weber in Ref. 1. This uses slender-wing theory to determine the load distribution and vortex drag, and not-so-slender theory to determine the lift-dependent wave drag. Theoretically these camber surfaces have attached flow at the leading edge at the design lift coefficient; for wings 6 and 7 this design C_L was 0·05. In addition the centre of pressure of wing 6 at $C_L = 0·05$ was fixed at 56·7% of the root chord and that of wing 7 at the same C_L at 49% of the root chord. These positions are determined by slender-wing theory and therefore apply only at low slenderness parameters (i.e. near $M = 1·0$); by the same theory the aerodynamic centre of the planform is at 56·3% of the root chord. Load distributions associated with the designs are shown in Fig. 5.

The camber surface of wing 8 was calculated by not-so-slender theory. In this calculation the design load distribution of wing 7, as found from slender-wing theory, was used in the not-so-slender theory to find a wing shape which would produce this load distribution at a slenderness parameter of 0·4 ($M \doteq 1·89$ for this planform). Thus, theoretically, the load distribution on wing 8 at $M = 1·89$ and $C_L = 0·05$ was the same as that on wing 7 at $M = 1·0$ and $C_L = 0·05$. The main

---

* Throughout this report the term camber is used to include both camber and twist.

† The word 'wing' is used to denote the theoretical shape whereas 'model' is used for the wing with sting shield. Similarly results which are influenced by this shield are termed 'model results' and results for which this influence is small, or absent, are termed 'wing results'.

4

differences in the calculated shapes of wings 7 and 8 occurred in the streamwise direction (*see* Ref. 3 for more details). Differences in spanwise shape were of the same order as the possible error of model manufacture. For simplicity therefore, these differences were ignored in the actual model construction and models 7 and 8 were made using the same spanwise templates, the chordwise datum of the templates being varied to allow for the differences in streamwise camber between the two models. In all the camber surfaces the wing trailing edge was straight.

The thickness distributions of the four wings were identical. The actual distribution was chosen to give low zero-lift drag, and pressure distributions sufficiently favourable (Fig. 6) to counteract the adverse gradients introduced by the wing camber (*see* Fig. 7 for some combined velocity distributions). It was also necessary to obtain a realistic value of the volume parameter, τ, $\{ = \text{volume}/(\text{wing area})^{3/2}\}$. These various requirements led to the use of an area distribution of the form

$$A\left(\frac{x}{c_0}\right) = K\left(\frac{x}{c_0}\right)^2 \left(1 - \frac{x}{c_0}\right).$$

For the uncambered wing the cross-sections normal to the stream direction were of rhombic form, the thickness/chord ratio of the centre section being $0 \cdot 065$. The surfaces of the cambered wings were found by simple addition of the ordinates of the uncambered-wing thickness distribution to the camber ordinates, i.e. the thickness was *not* added normal to the camber surface.

All the models were mounted in the tunnel on a sting-mounted strain-gauge balance. In order to shield the balance it was necessary to incorporate a small cylindrical body into the rear of the wing (Figs. 1 and 4). The axis of this body was parallel to the plane containing the wing apex and wing trailing edge. Because of mechanical difficulties in attaching the model to the balance it was not possible to make the bodies of the cambered models symmetrical with respect to the trailing edge (*see* Fig. 4).

All the wings were made of glass-cloth and an epoxy resin, formed over a metal core. This core was integral with the body and was used to make the model/balance joint.

3. Details of Tests.

3.1. Range of Tests.

The tests were made in the transonic and supersonic test sections of the 3 ft Tunnel at R.A.E., Bedford. Measurements were made of lift, drag and pitching moment in the nominal incidence* range $-2°$ to $+13°$ (one degree steps) at Mach numbers of $0 \cdot 4$, $0 \cdot 7$, $0 \cdot 9$, $0 \cdot 94$, $0 \cdot 98$, $1 \cdot 02$, $1 \cdot 42$, $1 \cdot 61$, $1 \cdot 82$ and $2 \cdot 00$. In addition surface oil-flow and vapour-screen patterns[8] were obtained at selected conditions; these conditions were chosen to cover test ranges in which the force results suggested changes in types of flow.

In all the force tests, bands of distributed roughness were used to ensure that the boundary layer on the model was turbulent on both surfaces of the wing (when the flow was not separated). They consisted of a mixture of carborundum grains and thin aluminium paint applied so that closely spaced individual grains projected from a paint base about $0 \cdot 001$ in. thick. At speeds up to $M = 1 \cdot 02$ the size of the particles used was $0 \cdot 003$ in. and at higher speeds $0 \cdot 007$ in. At all speeds the bands were half an inch wide (normal to the leading edge) and started $\frac{1}{8}$ in. inboard of the edge.

---

* For the cambered wings, incidence is defined as the incidence of the plane containing the wing apex and wing trailing edge.

A study of the oil-flow patterns and the drag results suggested that these roughness bands fixed transition downstream of the bands except for a small incidence range near the attached-flow condition at Mach numbers near $M = 1 \cdot 0$ and at $M = 2 \cdot 0$.

All the tests (except at $M = 2 \cdot 0$) were made at a constant Reynolds number of $1 \cdot 6 \times 10^6$ per foot. At $M = 2 \cdot 0$ the Reynolds number was reduced to $1 \cdot 35 \times 10^6$ per foot because of a limitation on tunnel power.

3.2. *Accuracy of Results.*

The balance results have been corrected for interaction effects and sting deflection before being reduced to coefficient forms: for all wings these coefficients are based on the dimensions of the basic wing planform. Moments are referred to the 40% point of the aerodynamic mean chord (that is, the moment centre is at $58 \cdot 4\%$ of the root chord). The drag has been corrected to a base pressure equal to free-stream static pressure. No correction has been applied for distortion caused by the sting-body. However, the possible errors due to the sting are discussed in more detail in an Appendix.

Incidence and pitching moment have been corrected for flow deflection and curvature in the tunnel stream. The flow corrections were found for the uncambered wing and the same corrections applied to all the cambered wings: the maximum corrections were $\Delta\alpha = 0 \cdot 1°$ and $\Delta C_m = 0 \cdot 0007$. Some spot checks on cambered wing 6 with the model inverted, showed that this method did not completely eliminate the errors but it is estimated that the residual errors are not greater than $\Delta\alpha = 0 \cdot 05°$ and $\Delta C_m = 0 \cdot 0003$. Measurements of C_{D0} in the normal and inverted case agreed to within $0 \cdot 0001$.

No corrections have been applied for wind-tunnel interference; this interference is, of course, absent at supersonic speeds when the bow shock wave is reflected clear of the model base ($M > 1 \cdot 3$). There is, however, some tunnel interference at subsonic and transonic speeds. Previous tests have shown that these effects are small except near $M = 1 \cdot 0$; here, however, the error in Mach number may be as large as $0 \cdot 02$, the free-stream Mach number being less than the tunnel Mach number.

Apart from this tunnel interference it is estimated that the accuracy of the results is as follows:

$$C_L \pm 0 \cdot 003$$
$$C_m \pm 0 \cdot 0006$$
$$C_D \pm 0 \cdot 0004 \text{ at } C_L = 0$$
$$\pm 0 \cdot 001 \text{ at } C_L = 0 \cdot 1$$
$$\alpha \pm 0 \cdot 05°.$$

4. *Discussion of Results.*

4.1. *Presentation of Results.*

The full set of force coefficients is tabulated in Tables 2 to 5. These results are plotted in Figs. 8 to 15 in the form of C_L against α and C_m against C_L and in Figs. 35 to 38 as C_D against C_L. It should be noted that the results presented have not been corrected for errors due to the sting shields. The magnitude of these errors is discussed in the Appendix where it is shown that the asymmetrical shields of *models* 6, 7 and 8 place additional lift near the model trailing edge, i.e. *wings* 6, 7 and 8 have less lift, and centres of pressure farther forward, than the tabulated results suggest: some effects of these corrections on the derived results are discussed in the next section. The asymmetrical stings appear to have only a small effect on the lift-dependent drag, but the shield volume does alter the level of the drag of all four wings as shown in Section 4.4.

6

Only a selection of the flow-visualization photographs (Figs. 29 to 33) are presented in this report; these, together with the force results, are discussed in the following sections.

4.2. Lift and Pitching Moment.

The curves of C_L against α, and of C_m against C_L plotted in Figs. 8 to 15 show most of the features now associated with the flow development over slender wings. In particular the results for the uncambered wing (wing 5) show that the lift-curve slope increases and the aerodynamic centre moves aft as the incidence is increased from zero. Similar increases in lift-curve slope, and rearward shifts in aerodynamic centre, are also present in the results for the cambered wings; however, for these wings the position of minimum lift-curve slope and of most forward position of aerodynamic centre is displaced to positive lift coefficients. It should be noted also that for all the cambered wings the aerodynamic centre is farthest forward (i.e. the wings are least stable) at low lift coefficients near $M = 1 \cdot 0$. This forward movement in aerodynamic centre takes place over a small range of C_L, thus causing a marked kink in the moment curves at low C_L.

The lift and moment results are now discussed in more detail with the aid of the derived results presented in Figs. 16 to 28. Fig. 16 shows the variation of lift with Mach number at fixed incidence: owing to the difficulty of defining a meaningful incidence for the cambered wings two sets of curves are presented. In the upper curves α is defined as the incidence of the plane containing the wing apex and the wing trailing edge (the usual incidence of this report). This figure compares the lift developed by the four wings when the height of the apex above the trailing edge is the same. The lower curve compares the lift when the local incidence at the centre of the trailing edge is the same. It will be seen that when the lift is compared at constant apex height (Fig. 16a) the cambered wings produce less lift than the uncambered wings. On the other hand, when the lift is compared at constant trailing-edge incidence (Fig. 16b) the lifts of all four wings are much closer together, although at subsonic speeds the cambered wings again produce less lift than the uncambered wing. This loss of lift by the cambered wings, relative to the plane wing, is caused by two main effects, the positive zero-lift angle and the delay to higher lift coefficients of the onset of non-linear lift. In addition the actual strength of this non-linear lift affects the results.

The development of non-linear lift is examined further in Fig. 17 where curves of $(C_L - \bar{C}_L)$ against $(\alpha - \bar{\alpha})$ are presented for two subsonic and two supersonic Mach numbers. $\bar{\alpha}$ is defined as the incidence at which the lift-curve slope is a minimum and $\bar{C}_L$ is the corresponding value of C_L. $\bar{\alpha}$ was found from plots of $\partial C_L / \partial \alpha$ against α (typical plots are shown in Fig. 18) and the variations of $\bar{\alpha}$, $\bar{C}_L$ and $\bar{C}_m$ (value of C_m at $\bar{C}_L$) with Mach number are shown in Figs. 20 to 22. The choice of incidence datum as the incidence at which the lift-curve slope is a minimum is based on the assumption that the flow was attached at the leading edge when this occurred, a fact which can be confirmed from the flow-visualization results (Section 4.3).

From Fig. 17 it can be seen that at each Mach number the cambered-wing results collapse onto a single curve which lies slightly above the uncambered-wing results at higher incidence, although at $\alpha = \bar{\alpha}$ the lift-curve slope of all four wings is the same. This suggests that the vortex and non-linear lift development are the same on all the cambered wings; the strength of the vortex being greater than on the plane wing. The larger non-linear lift is also shown in Fig. 19 where $\partial C_L / \partial \alpha$ at $\alpha = \bar{\alpha}$, $\alpha = \bar{\alpha} + 5°$ and $\alpha = \bar{\alpha} - 5°$ is plotted against Mach number: the increase in slope between $\bar{\alpha}$ and $\bar{\alpha} + 5°$ is clearly greater for the cambered wings. For all the wings the non-linear lift at $M = 1 \cdot 0$ is larger than the value $4\alpha^2$ predicted by Smith[10].

7

In the analysis of moment results we are mainly interested in the following three aspects:

(i) The effects of camber on centre-of-pressure position and on stability.

(ii) Comparison of the experimental results with design values.

(iii) Effects of camber on trim.

Figs. 23 and 24 show the variations of centre of pressure and aerodynamic centre with Mach number at constant C_L. These results show that, in general, a forward movement in centre-of-pressure position for the cambered wings is associated with a corresponding forward shift in aerodynamic centre relative to that of the plane wing. However, it should be noted that the effect of flow separation is to move the aerodynamic centre aft, so that some of the differences between the positions of aerodynamic centre of the cambered and uncambered wings at fixed C_L are due to differences in the flow development at C_L. Fig. 25 shows typical plots of $(C_m - \bar{C}_m)$ against $(C_L - \bar{C}_L)$; these show that even at equal values of $(C_L - \bar{C}_L)$ the cambered wings tend to be less stable than the uncambered wing.

No corrections for possible sting effects have been applied to the results presented in Fig. 23; thus these results should not be directly compared with the design parameters. This comparison is made in Fig. 26 where the corrected centre-of-pressure positions at design Mach number and lift coefficient are plotted against the theoretical position. (In addition to the design positions, the centre-of-pressure positions of wing 8 at $C_L = 0\cdot05$, $M = 1\cdot0$ and wing 7 at $C_L = 0\cdot05$, $M = 1\cdot89$ were found during the design of wing 8, and measured positions corresponding to these conditions are included in Fig. 26.) The corrected positions at $M = 1\cdot0$ vary linearly with the theoretical position, but are between 2% and 5% centre-line chord nearer the apex. It should be noted that the measured positions of centre of pressure at $M = 1\cdot0$ for two of the cambered gothic wings tested previously (Ref. 5) also lie on this line. Since the sting shields of these models are symmetrical these results do not require a sting correction and so it may be assumed that the trend shown in Fig. 26 is genuine. At $M = 1\cdot89$ the corrected positions are close to the theoretical positions.

As a measure of the effectiveness of camber in trimming the models at supersonic speeds, curves showing the trim C_L for two possible centre-of-gravity positions are shown in Fig. 27. The two positions of centre of gravity have been chosen to coincide with the most forward aerodynamic-centre positions occurring on the cambered wings at low speeds ($M = 0\cdot4$) and transonic speeds ($M = 0\cdot98$ and $1\cdot02$) respectively. These positions are:

	$M = 0\cdot4$	$M = 0\cdot98, 1\cdot02$
Wing 6	$0\cdot545c_0$	$0\cdot510c_0$
Wing 7	$0\cdot550c_0$	$0\cdot520c_0$
Wing 8	$0\cdot550c_0$	$0\cdot535c_0$

The final figure (Fig. 28) of this part of the analysis shows the variation of aerodynamic-centre position and lift-curve slope at zero incidence of wing 5 with Mach number and compares experiment with theory for $M > 1$. At low supersonic speeds the theoretical variation is based on not-so-slender theory[3], whereas at Mach numbers above $M = 1\cdot3$ the theoretical curve is based on linear theory, but applied to a cropped delta[6] with the same apex angle and aspect ratio as the true wing. It will be seen that the experimental points follow the theoretical trends, but the aerodynamic centre is about 1% c_0 farther aft, and the lift-curve slope about 10% lower, than the theories predict.

8

4.3. *Flow Development.*

Typical surface oil-flow and vapour-screen photographs illustrating the main features of the flow development over wings 5 and 7 are presented in Figs. 29 to 33

The main purpose of the flow-visualization tests was to study the onset and development of leading-edge separations. The roughness bands tended to hide some of these features and so were removed: however, some early tests with and without roughness showed that the separated flow inboard of the bands was independent of roughness.

The photographs of the flow development over wing 5 at $M = 1\cdot61$ (Figs. 29 and 30) show that at all positive incidences the flow separates from part, or all, of the leading edge, and forms a vortex above the wing. Traces of this separation are clearly shown in the vapour screen at $0\cdot3°$ incidence and the surface flow pattern at $1\cdot3°$ shows leading-edge separation taking place over the rear 70% or so of the edge. With increase in incidence the separation spreads to the apex and the vortex increases in strength and moves inboard. As the vortex strength increases the spanwise flow separates and the vortex sheet from this separation eventually rolls up into a second vortex under the main vortex. The oil pattern associated with this vortex system can be seen at $\alpha = 8\cdot6°$, and the secondary separation is clearly visible* in the vapour-screen photographs at incidences above $5\cdot5°$. The dark circular region above the wing in the vapour screen is believed to be a fair representation of the vortex core; if this is so, then the height of this core above the wing surface is approximately half the height predicted by Smith's calculations[10] based on slender-wing theory. This tendency of the vortex core to move closer to the wing with increase in Mach number is discussed in Ref. 9.

The surface flow over the three cambered wings was investigated at a series of incidences at $M = 1\cdot61$ and $2\cdot0$. In general the flow development was virtually the same over all three cambered wings: hence only one case, that of wing 7, is exhibited. Upper-surface flow patterns for this wing at $M = 1\cdot61$ and $2\cdot0$ are presented in Figs. 31 and 33 and vapour-screen photographs at $M = 1\cdot6$ in Fig. 32. At $M = 1\cdot61$ and at incidences below $\alpha = 5$ the flow was attached over the upper surface and a vortex occurred along part, or all, of the lower-surface leading edge. The upper-surface pattern at $5\cdot44°$ incidence suggests that leading-edge separation occurs near the wing tip, a fact which is confirmed by the vapour screen at this incidence. As the incidence increases above $5\cdot44°$ the vortex again moves inboard and increases in strength but the oil patterns suggest that the secondary separation is nearer the edge than on the plane wing at equal incidences above the start of separation. Also, although this depends on the exact interpretation of the vapour screen, the vortex core appears more oval shaped, and closer to the wing surface on the cambered wing. These differences could account for the higher non-linear lift of the cambered wings relative to the plane wing.

In general the oil-flow patterns at $M = 2\cdot0$ suggest that the flow remains attached over the upper surface to a higher incidence than at $M = 1\cdot61$ and that even when the flow does separate, the surface flow is much less well defined than at $M = 1\cdot61$. Also at $\alpha = 10\cdot09°$ incidence the surface oil pattern near the leading edge has a wavy form. This type of oil pattern was also found in a study of the flow over some delta wings (Ref. 9), and it was shown that it corresponds to an array of streamwise vortices in the separated vortex sheet: the wavy form occurring in the oil pattern when this sheet is near the wing surface. Thus it appears that as the Mach number increases to $M = 2\cdot0$ the vortex sheet moves closer to the wing surface. (It was not possible in this series of tests to obtain a vapour screen at $M = 2\cdot0$.)

---

* For a fuller discussion of the interpretation of the vapour screen see Refs. 8 and 9.

The results of the total flow-visualization programme at supersonic speeds is summarised in Fig. 34 in the form of plots of attachment-line position* against $\alpha - \bar{\alpha}$. It will be seen that for all wings at both Mach numbers the attachment line appears to reach the leading edge at, or near, $\alpha = \bar{\alpha}$. Thus we may assume that $\bar{\alpha}$, which is the incidence corresponding to minimum lift-curve slope, is also the incidence at which the flow is attached over the whole wing. All the cambered wings were designed to have attached flow at the leading edge at the design conditions; hence it is of interest to compare the measured values of $\bar{\alpha}$ and $\bar{C}_L$ (Figs. 20 and 21) at the design Mach number with the design values. The results are given in the following table.

	$(\alpha)_d$	$(C_L)_d$	$(M)_d$	$\bar{\alpha}$	$\bar{C}_L$
Wing 6	$3 \cdot 09°$	$0 \cdot 05$	$1 \cdot 0$	$3 \cdot 9°$	$0 \cdot 06$
Wing 7	$4 \cdot 74°$	$0 \cdot 05$	$1 \cdot 0$	$4 \cdot 8°$	$0 \cdot 05_5$
Wing 8	$4 \cdot 97°$	$0 \cdot 05$	$1 \cdot 89$	$5 \cdot 5°$	$0 \cdot 07$

It will be seen that only for model 7 are the experimental and design values in good agreement. The results for model 8 are particularly disappointing in that although $\bar{\alpha}$ is only $0 \cdot 5°$ above $\alpha = \bar{\alpha}$, $\bar{C}_L$ is $0 \cdot 02$ higher than $(C_L)_d$.

In addition to the flow-visualization tests discussed above, some flow studies were made at subsonic and transonic speeds. At $M = 0 \cdot 70$ the vortex above wing 5 appeared to be nearer the leading edge than at the same incidence at $M = 1 \cdot 61$, also at the same values of $\alpha - \bar{\alpha}$ the surface flow patterns on wings 5 and 7 were almost identical. The transonic flow pictures, which were taken in an attempt to find causes of the forward movement of aerodynamic centre in this speed range at low C_L, did not reveal any unusual features; in particular there were no signs of shock waves in the surface flow patterns and the vortex development appeared the same as at other Mach numbers. Thus the forward movement in aerodynamic centre is not caused by boundary-layer separations induced by the trailing-edge shock: but more likely by changes in the pressure field near the trailing edge as the trailing-edge shock is established.

4.4. Drag.

Drag polars for the four models are plotted in Figs. 35 to 38. In Figs. 39 and 40 the results are cross-plotted as curves of C_D against Mach number for fixed C_L. These curves show that above $C_L \doteq 0 \cdot 1$ all the cambered models have lower drag than the plane model, thus the trim associated with the camber has been obtained without any large drag penalty.

For a more detailed analysis of the drag results we divide the drag into a thickness, or volume, drag and a lift-dependent drag. The volume drag is defined as the zero-lift drag of the plane wing, and this is compared with theoretical estimates in Fig. 41. The theoretical drag consists of the supersonic wave drag of the model as calculated by slender-body theory, together with a skin-friction drag calculated by a strip theory using flat-plate turbulent boundary layers. The measured points are in good agreement with theoretical estimates, except at $M = 2 \cdot 0$ where the measured point is low relative to theory and relative also to the trend of the other experimental points. It is thought that this particular discrepancy is caused by a partial failure of the transition band at $M = 2 \cdot 0$.

---

* The attachment line in the vapour screen is taken as the inner edge of the dark region above the wing.

The lift-dependent drag has been analysed in terms of a lift-dependent drag factor, $K = \pi A(C_D - C_{D0})/C_L^2$. This factor is plotted in Figs. 42 and 43 against C_L and against $\beta s_T/c_0$. In this factor C_{D0} is the volume drag and so is equal to the zero-lift drag of the uncambered wing*.

In general it appears that the lift-dependent drag increases with forward movement of the design centre of pressure, i.e. wing 8 has the highest lift-dependent drag. This effect is most marked at low C_L, but at supersonic speeds and at values of C_L above $0 \cdot 1$ the lift-dependent drag of all the cambered models is approximately the same and is less than that of the uncambered wing.

Fig. 43 shows that the lift-dependent drag is a minimum at low supersonic speeds. Above $M = 1 \cdot 4$ the increase can be expressed in the form $K = K_v + 2(\beta s_T/c_0)^2 K_w$; values of K_v and K_w for the various models are:

Model	K_v	K_w
5	1·3	1·3
6	1·3	1·0
7	1·2	1·4
8	1·4	1·0

In Figs. 44 and 45 the tunnel values of $(L/D)_{max}$ and C_L for $(L/D)_{max}$ are plotted against Mach number for supersonic speeds. These figures show that camber increases the maximum values of L/D by about $0 \cdot 2$. When assessing these gains it must be remembered that wings 5 and 6 are untrimmed whereas wing 7 is trimmed at a C_L of about $0 \cdot 05$ and wing 8 at a C_L of at least $0 \cdot 075$ (Fig. 27). Thus the camber surfaces of wings 7 and 8 have produced a slight increase in $(L/D)_{max}$ relative to the uncambered wing together with a trimmed wing at a reasonable C_L. Extrapolating to full-scale conditions and allowing for the effect of sting distortion gives full-scale values of $(L/D)_{max}$ which are about $0 \cdot 5$ higher than those plotted in Fig. 44 for $M = 1 \cdot 4$ and about $0 \cdot 9$ higher at $M = 2 \cdot 0$.

5. Conclusions.

From these tests on cambered gothic wings, designed to provide a low-drag method of trimming the rearward shift in aerodynamic centre which occurs between subsonic and supersonic speeds, the following conclusions can be drawn.

(a) At the design conditions the centre of pressure is close to, or slightly ahead, of the design position. In the case of those designed by slender-wing theory, trimming power associated with the forward position of centre of pressure (relative to the aerodynamic centre) at the design Mach number ($M = 1 \cdot 0$) shows only a slight fall off with increase in Mach number.

(b) The cambered wings, which are trimmed at some positive C_L, have maximum lift/drag ratios which are just above those of the plane wing.

(c) When the lift of the four wings is compared at constant trailing-edge incidence the cambered wings produce about the same lift as the uncambered wing at supersonic speeds, and slightly less at subsonic speeds.

---

* The measured values of C_{D0} at $M = 2 \cdot 0$ and near $M = 1 \cdot 0$ have been given a minor adjustment to allow for the partial failure of transition bands at these speeds.

(*d*) On all the wings there is an incidence, depending on Mach number, at which the flow is attached over the whole wing, and at which the lift-curve slope is a minimum and the aerodynamic centre farthest forward. Away from this attachment point the lift-curve slope increases and the aerodynamic centre moves aft. These two effects decrease with increase in Mach number above $M = 1 \cdot 0$, but the decrease is less marked for the cambered wings than for the uncambered wing. Also at all speeds the non-linear lift developed by the cambered wings is greater than that developed by the uncambered wing.

(*e*) Near $M = 1 \cdot 0$ there is a marked forward movement of aerodynamic centre on the cambered wings; this forward movement is confined to a small C_L range near the attachment point.

LIST OF SYMBOLS

A	Aspect ratio
c_0	Root chord
$\bar{c}$	Aerodynamic mean chord
C_D	Drag coefficient $= \mathrm{drag}/qS$
C_L	Lift coefficient $= \mathrm{lift}/qS$
C_m	Pitching-moment coefficient $= \mathrm{pitching\ moment}/qS\bar{c}$
M	Mach number
p	Planform parameter $= S/2s_T c_0$
q	Kinetic pressure
S	Wing area
s_T	Semi-span at trailing edge
$s(x)$	Equation of leading edge
V	Wing volume
V_0	Free-stream velocity
v_x	Perturbation velocity in x-direction
x, y, z	Co-ordinates (*see* Fig. 1)
α	Wing incidence (For the cambered wings incidence is based on the incidence of the plane containing the wing apex and wing trailing edge.)
β	$= (M^2-1)^{1/2}$ or $(1-M^2)^{1/2}$
η	$= y/s(x)$
τ	Volume parameter $V/S^{3/2}$
βs_T	Slenderness parameter

13

REFERENCES

No.	Author(s)	Title, etc.

1 J. Weber .. .. — Design of warped slender wings with the attachment line along the leading edge.
A.R.C. 20 051. September, 1957.

2 E. C. Maskell and J. Weber .. — On the aerodynamic design of slender wings.
J. R. Ae. Soc., Vol. 63, No. 588, pp. 709 to 721. December, 1959.

3 L. C. Squire .. .. .. — Some applications of 'not-so-slender' wing theory to wings with curved leading edges.
A.R.C. R. & M. 3278. July, 1960.

4 L. C. Squire .. .. .. — An experimental investigation at supersonic speeds of the characteristics of two gothic wings, one plane and one cambered.
A.R.C. R. & M. 3211. May, 1959.

5 L. C. Squire .. .. .. — Further experimental investigations of the characteristics of cambered gothic wings at Mach numbers from 0·4 to 2·0.
A.R.C. R. & M. 3310. December, 1961.

6 J. H. B. Smith, J. A. Beasley and A. Stevens. — Calculations of the lift slope and aerodynamic centre of cropped delta wings at supersonic speeds.
A.R.C. C.P. 562. July, 1960.

7 R. F. A. Keating .. .. .. — Low-speed wind-tunnel tests on sharp-edged gothic wings of aspect-ratio 3/4.
A.R.C. C.P. 576. May, 1960.

8 I. McGregor .. .. .. — Development of the vapour screen method of flow visualisation in the 3 ft × 3 ft tunnel at R.A.E., Bedford.
J. Fluid Mech., Vol. 11, p. 481. 1961.

9 L. C. Squire, J. G. Jones and A. Stanbrook. — An experimental investigation of the characteristics of some plane and cambered 65° delta wings at Mach numbers from 0·7 to 2·0.
A.R.C. R. & M. 3305. July, 1961.

10 J. H. B. Smith .. .. .. — A theory of the separated flow from the curved leading edge of a slender wing.
A.R.C. R. & M. 3116. November, 1957.

11 B. W. Bolton Shaw .. .. — Nose controls on delta wings at supersonic speeds.
College of Aeronautics Report No. 36.
A.R.C. 13 372. May, 1950.

APPENDIX

Effect of Sting Shields

As pointed out in Section 2 it was not possible to make the sting shields on the cambered wings symmetrical with respect to the trailing edge (Figs. 2 and 4). In fact on all the cambered models the larger part of the shield is on the lower surface of the wing and it would be expected that the differences in the pressure fields of the two parts of the shield would produce a positive lift near the trailing edge. In this Appendix the magnitude of this lift is calculated by assuming that the effect of the asymmetrical sting can be found by regarding it as equivalent to an additional camber (based on the mean of the upper and lower surfaces of the exposed body) plus a thickness effect. From the shield geometry shown in Fig. 4, it will be seen that this additional camber surface effectively increases the wing incidences in the region masked by the shield. The increase in incidence is approximately constant over most of this region dropping rapidly to zero near the shield/wing junction. For wings 7 and 8 the increase is about $0 \cdot 045$ radians and for wing 6, $0 \cdot 009$ radians.

At $M = 1 \cdot 0$ the lift due to this additional incidence can be calculated by slender-wing theory. The increase in C_L for models 7 and 8 is $0 \cdot 009$ and this load acts near the centre of the shield, thus C_m is decreased by $0 \cdot 003$. Applying these corrections to the measured results at $M = 0 \cdot 98$ and $1 \cdot 02$ we find that the presence of the sting increases C_L by $0 \cdot 009$ decreases $(C_m)_0$ by $0 \cdot 0027$.

At $M = 2 \cdot 0$ the sting shield only influences a region inside the Mach cone from the apex of the sting and if it is assumed that the surface masked by the shield is conical, then the forces can be calculated by linear theory. In fact they can be found directly from the analysis of Ref. 11, giving for models 7 and 8, $\Delta C_L = 0 \cdot 004$, $\Delta C_m = -0 \cdot 0017$. These increments correspond to an increase in the $(C_m)_0$ of the wing alone of $0 \cdot 0014$. The magnitude of these corrections was confirmed by integration of the pressure fields of half cores on the upper and lower surfaces with base areas equal to the shield base areas.

The presence of the stings affects the drag measurements in two ways. The additional volume affects the zero-lift drag of all the models (this effect is discussed in Section 4.4) and the asymmetry affects the lift-dependent drag. This latter effect has been calculated at $M = 2 \cdot 0$ using the values of ΔC_L calculated above. It was found that the maximum effect at $C_L = 0 \cdot 10$ was to decrease the drag by $0 \cdot 00015$ for wings 7 and 8, i.e. the true lift-dependent drag factor at $C_L = 0 \cdot 10$ could be $0 \cdot 04$ higher than the quoted values.

TABLE 1

Details of Models

(a) *Planform* (*All Wings*).

Equation of leading edge $y = s(x) = s_T \left(\dfrac{x}{c_0}\right) \left\{ 1 \cdot 25 - 0 \cdot 25 \left(\dfrac{x}{c_0}\right)^4 \right\}$

c_0 (root chord)	$= 22$ inches
s_T (semi-span at trailing edge)	$= 5 \cdot 5$ inches
$\bar{c}$ (aerodynamic mean chord)	$= 15 \cdot 265$ inches
S (wing area)	$= 141 \cdot 167$ inches
Aspect ratio	$= 6/7$
$p \; (= S/2c_0 s_T)$	$= 7/12.$

(b) *Cross-Sectional Area Distribution* (*All Wings*) *Excluding Sting Fairing*.

$S(x)$	$= 0 \cdot 080176 c_0{}^2 \left(\dfrac{x}{c_0}\right)^2 \left(1 - \dfrac{x}{c_0}\right)$
V (wing volume)	$= 0 \cdot 006681 c_0{}^3$
$\tau \; (= V/S^{3/2})$	$= 0 \cdot 0424.$

(c) *Wing Ordinates.*

Uncambered wing (wing 5)

$$Z_5(x, y) = \pm \tfrac{1}{2}(S(x)/s(x)) \left(1 - \left| \dfrac{y}{s(x)} \right| \right).$$

Cambered wings

$$Z_i(x, y) = \int_{c_0}^{x} \dfrac{\partial Z_i(x, y)}{\partial x} \pm Z_5(x, y)$$

where

Wing 6
$$\begin{cases}
\dfrac{\partial Z_6(x, y)}{\partial x} = -0 \cdot 04312 \left(1 \cdot 5 - 0 \cdot 5 \dfrac{x}{c_0}\right) & \text{for } 0 \leqslant |\eta| \leqslant \eta_0(x) \\[3mm]
\quad = -0 \cdot 04312 \left(1 \cdot 5 - 0 \cdot 5 \dfrac{x}{c_0}\right) \left[1 - \dfrac{\pi(|\eta| - \eta_0)^2}{(1 + 2\eta_0{}^2)\cos^{-1}\eta_0 - 3\eta_0 \sqrt{(1 - \eta_0{}^2)}} \right] \\[2mm]
\qquad\qquad\qquad\qquad\qquad\qquad\qquad\quad \text{for } \eta_0(x) \leqslant |\eta| \leqslant 1 \\[3mm]
\left(\eta = y/s(x), \quad \eta_0(x) = 0 \cdot 75 \dfrac{x}{c_0} \right)
\end{cases}$$

Wing 7
$$\begin{cases}
\dfrac{\partial Z_7(x, y)}{\partial x} = -0 \cdot 04312 \, (3 \cdot 5 - 4 \cdot 5x + 2x^2) & \text{for } 0 \leqslant |\eta| \leqslant \eta_0(x) \\[3mm]
\quad = -0 \cdot 04312 \, (3 \cdot 5 - 4 \cdot 5x + 2x^2) \left[1 - \dfrac{\pi(|\eta| - \eta_0)^2}{(1 + 2\eta_0{}^2)\cos^{-1}\eta_0 - 3\eta_0 \sqrt{(1 - \eta_0{}^2)}} \right] \\[2mm]
\qquad\qquad\qquad\qquad\qquad\qquad\qquad\quad \text{for } \eta_0(x) \leqslant |\eta| \leqslant 1 \\[3mm]
\left(\eta = y/s(x), \quad \eta_0(x) = 0 \cdot 75 \dfrac{x}{c_0} \right)
\end{cases}$$

Wing 8 $\quad \dfrac{\partial Z_8(x, y)}{\partial x} = \dfrac{\partial Z_7(x, y)}{\partial x} + \dfrac{\partial(\Delta Z)}{\partial x}.$

(There is no explicit formula for ΔZ, details are given in Ref. 3.)

TABLE 2

Aerodynamic Coefficients of Model 5

M	$\alpha°$	C_L	C_m	C_D	M	$\alpha°$	C_L	C_m	C_D
0·40	− 2·09	−0·048	−0·0009	0·0095	0·70	− 2·02	−0·049	−0·0007	0·0095
	− 1·08	−0·023	−0·0009	0·0084		− 1·09	−0·025	−0·0005	0·0085
	− 0·06	−0·002	−0·0001	0·0077		− 0·06	−0·002	0·0000	0·0076
	+ 0·96	+0·021	+0·0006	0·0082		+ 0·97	+0·021	+0·0005	0·0082
	+ 1·98	+0·046	+0·0009	0·0093		+ 1·99	+0·047	+0·0006	0·0093
	+ 3·00	+0·075	+0·0011	0·0116		+ 3·03	+0·076	+0·0007	0·0113
	+ 4·02	+0·106	+0·0014	0·0145		+ 4·07	+0·108	+0·0007	0·0147
	+ 5·04	+0·136	+0·0018	0·0186		+ 5·11	+0·140	+0·0006	0·0189
	+ 6·07	+0·171	+0·0021	0·0243		+ 6·15	+0·175	+0·0004	0·0248
	+ 7·09	+0·207	+0·0023	0·0311		+ 7·19	+0·212	+0·0001	0·0319
	+ 8·12	+0·244	+0·0026	0·0397		+ 8·23	+0·250	+0·0002	0·0411
	+ 9·15	+0·284	+0·0029	0·0499		+ 9·28	+0·295	−0·0004	0·0525
	+10·18	+0·323	+0·0036	0·0613		+10·33	+0·337	−0·0007	0·0651
	+11·21	+0·363	+0·0043	0·0746		+11·38	+0·383	−0·0009	0·0799
	+12·25	+0·405	+0·0049	0·0897		+12·43	+0·428	−0·0010	0·0966
	+13·29	+0·460	+0·0051	0·1094		+13·49	+0·474	−0·0012	0·1154
0·90	− 2·13	−0·051	−0·0003	0·0098	0·94	− 2·13	−0·052	−0·0003	0·0099
	− 1·09	−0·025	−0·0005	0·0084		− 1·10	−0·026	−0·0005	0·0085
	− 0·06	−0·002	+0·0001	0·0073		− 0·06	−0·001	+0·0001	0·0074
	+ 0·98	+0·022	+0·0007	0·0082		+ 0·98	+0·022	+0·0007	0·0082
	+ 2·01	+0·049	+0·0006	0·0094		+ 2·02	+0·050	+0·0005	0·0094
	+ 3·05	+0·079	+0·0003	0·0115		+ 3·06	+0·081	+0·0003	0·0117
	+ 4·10	+0·113	−0·0002	0·0150		+ 4·10	+0·115	−0·0004	0·0153
	+ 5·14	+0·148	−0·0010	0·0197		+ 5·14	+0·150	−0·0015	0·0200
	+ 6·18	+0·186	−0·0021	0·0260		+ 6·19	+0·188	−0·0029	0·0263
	+ 7·23	+0·227	−0·0036	0·0341					
	+ 8·28	+0·271	−0·0050	0·0445		+ 8·28	+0·275	−0·0066	0·0454
	+ 9·33	+0·315	−0·0061	0·0565		+ 9·34	+0·318	−0·0081	0·0575
	+10·38	+0·356	−0·0075	0·0695		+10·38	+0·363	−0·0102	0·0714
	+11·44	+0·402	−0·0091	0·0853		+11·44	+0·410	−0·0123	0·0875
	+12·50	+0·451	−0·0111	0·1034		+12·49	+0·459	−0·0150	0·1059
	+13·55	+0·496	−0·0123	0·1228		+13·55	+0·507	−0·0173	0·1260
0·98	− 2·13	−0·053	−0·0006	0·0103	1·02	− 2·13	−0·055	+0·0013	0·0132
	− 1·10	−0·025	−0·0009	0·0088		− 1·09	−0·027	0·0000	0·0120
	− 0·06	−0·001	0·0000	0·0077		− 0·06	−0·002	0·0000	0·0109
	+ 0·98	+0·022	+0·0006	0·0085		+ 0·98	+0·023	+0·0001	0·0119
	+ 2·02	+0·050	+0·0004	0·0097					
	+ 3·06	+0·081	−0·0002	0·0121		+ 3·05	+0·086	−0·0025	0·0156
	+ 4·11	+0·117	−0·0013	0·0158		+ 4·09	+0·121	−0·0041	0·0191
	+ 5·15	+0·153	−0·0028	0·0208		+ 5·13	+0·158	−0·0064	0·0243
	+ 6·19	+0·194	−0·0052	0·0276		+ 6·17	+0·200	−0·0101	0·0318
	+ 7·23	+0·239	−0·0084	0·0366		+ 7·21	+0·246	−0·0139	0·0410
	+ 8·28	+0·282	−0·0110	0·0472		+ 8·25	+0·287	−0·0166	0·0510
	+ 9·32	+0·326	−0·0136	0·0597		+ 9·29	+0·330	−0·0196	0·0633
	+10·37	+0·373	−0·0172	0·0743		+10·34	+0·376	−0·0228	0·0777
	+11·41	+0·420	−0·0206	0·0909		+11·38	+0·423	−0·0271	0·0943
	+12·46	+0·467	−0·0243	0·1093		+12·42	+0·469	−0·0310	0·1127
	+13·50	+0·517	−0·0291	0·1303		+13·47	+0·517	−0·0347	0·1333

B

TABLE 2—*continued*

Aerodynamic Coefficients of Model 5

M	$\alpha°$	C_L	C_m	C_D	M	$\alpha°$	C_L	C_m	C_D
1·42	− 1·95	−0·052	+0·0033	0·0136	1·61	− 1·75	−0·040	+0·0026	0·0122
	− 0·92	−0·024	+0·0014	0·0124		− 0·72	−0·014	+0·0009	0·0114
	+ 0·11	+0·002	−0·0001	0·0121		+ 0·31	+0·010	−0·0006	0·0113
	+ 1·14	+0·027	−0·0016	0·0127		+ 1·34	+0·035	−0·0024	0·0121
	+ 2·17	+0·056	−0·0036	0·0138		+ 2·36	+0·063	−0·0045	0·0136
	+ 3·20	+0·086	−0·0058	0·0162		+ 3·39	+0·091	−0·0068	0·0161
	+ 4·23	+0·118	−0·0081	0·0198		+ 4·42	+0·121	−0·0091	0·0195
	+ 5·27	+0·151	−0·0106	0·0246		+ 5·46	+0·152	−0·0115	0·0244
	+ 6·30	+0·185	−0·0131	0·0305		+ 6·49	+0·184	−0·0140	0·0303
	+ 7·35	+0·224	−0·0160	0·0384		+ 7·53	+0·219	−0·0166	0·0378
	+ 8·38	+0·258	−0·0187	0·0474		+ 8·56	+0·252	−0·0191	0·0465
	+ 9·42	+0·295	−0·0218	0·0582		+ 9·60	+0·284	−0·0216	0·0564
	+10·46	+0·331	−0·0247	0·0703		+10·63	+0·318	−0·0245	0·0680
	+11·50	+0·367	−0·0274	0·0837		+11·67	+0·351	−0·0273	0·0809
	+12·54	+0·405	−0·0304	0·0991		+12·71	+0·382	−0·0298	0·0945
	+13·58	+0·442	−0·0334	0·1155		+13·74	+0·417	−0·0326	0·1103
1·82	− 1·90	−0·046	+0·0029	0·0121	2·00	− 2·19	−0·051	+0·0033	0·0118
	− 0·88	−0·021	+0·0011	0·0110		− 1·22	−0·026	+0·0016	0·0102
	+ 0·15	+0·003	−0·0004	0·0106		− 0·15	−0·003	+0·0003	0·0093
	+ 1·18	+0·027	−0·0020	0·0112		+ 0·87	+0·020	−0·0010	0·0098
	+ 2·21	+0·053	−0·0039	0·0126		+ 1·90	+0·044	−0·0027	0·0113
	+ 3·23	+0·080	−0·0059	0·0149		+ 2·92	+0·069	−0·0044	0·0134
	+ 4·26	+0·109	−0·0081	0·0181		+ 3·94	+0·095	−0·0064	0·0162
	+ 5·30	+0·138	−0·0103	0·0225		+ 4·97	+0·122	−0·0083	0·0201
	+ 6·33	+0·167	−0·0126	0·0279		+ 5·99	+0·150	−0·0103	0·0250
	+ 7·36	+0·201	−0·0151	0·0347		+ 7·02	+0·178	−0·0125	0·0307
	+ 8·40	+0·231	−0·0174	0·0425		+ 8·04	+0·206	−0·0146	0·0377
	+ 9·43	+0·263	−0·0198	0·0518		+ 9·07	+0·238	−0·0169	0·0462
	+10·46	+0·292	−0·0221	0·0621		+10·10	+0·266	−0·0189	0·0554
	+11·50	+0·323	−0·0246	0·0739		+11·13	+0·294	−0·0211	0·0659
	+12·53	+0·354	−0·0272	0·0868		+12·15	+0·322	−0·0233	0·0774
						+13·18	+0·349	−0·0253	0·0899

TABLE 3

Aerodynamic Coefficients of Model 6

M	$\alpha°$	C_L	C_m	C_D	M	$\alpha°$	C_L	C_m	C_D
0·40	− 2·10	−0·102	+0·0048	+0·0174	0·70	− 2·18	−0·104	+0·0057	+0·0179
	− 1·13	−0·073	+0·0048	+0·0141		− 1·20	−0·073	+0·0052	+0·0144
	− 0·06	−0·042	+0·0047	+0·0117		− 1·12	−0·042	+0·0048	+0·0118
	+ 0·96	−0·014	+0·0047	+0·0100		+ 0·91	−0·012	+0·0045	+0·0098
	+ 1·98	+0·013	+0·0044	+0·0090		+ 1·94	+0·015	+0·0043	+0·0090
	+ 2·99	+0·037	+0·0046	+0·0088		+ 2·97	+0·039	+0·0043	+0·0085
	+ 4·01	+0·059	+0·0056	+0·0102		+ 4·00	+0·060	+0·0055	+0·0099
	+ 5·03	+0·082	+0·0069	+0·0116		+ 5·04	+0·084	+0·0066	+0·0115
	+ 6·06	+0·109	+0·0081	+0·0137		+ 6·07	+0·114	+0·0074	+0·0141
	+ 7·08	+0·138	+0·0086	+0·0173		+ 7·11	+0·145	+0·0076	+0·0180
	+ 8·10	+0·170	+0·0092	+0·0221		+ 8·15	+0·179	+0·0078	+0·0234
	+ 9·13	+0·207	+0·0098	+0·0286		+ 9·19	+0·215	+0·0082	+0·0299
	+10·16	+0·241	+0·0104	+0·0359		+10·24	+0·256	+0·0085	+0·0388
	+11·19	+0·283	+0·0106	+0·0463		+11·29	+0·296	+0·0089	+0·0493
	+12·22	+0·325	+0·0116	+0·0582		+12·34	+0·339	+0·0089	+0·0622
	+13·25	+0·364	+0·0123	+0·0710		+13·40	+0·387	+0·0095	+0·0777
0·90	− 2·19	−0·108	+0·0077	+0·0181	0·94	− 2·14	−0·110	+0·0084	+0·0180
	− 1·15	−0·076	+0·0067	+0·0143		− 1·15	−0·077	+0·0072	+0·0144
	− 0·12	−0·043	+0·0058	+0·0115		− 0·06	−0·044	+0·0061	+0·0115
	+ 0·92	−0·012	+0·0050	+0·0096		+ 0·97	−0·013	+0·0052	+0·0095
	+ 1·96	+0·017	+0·0045	+0·0086		+ 2·02	+0·016	+0·0046	+0·0086
	+ 2·99	+0·042	+0·0046	+0·0084		+ 3·07	+0·043		+0·0080
	+ 4·03	+0·064	+0·0061	+0·0099		+ 4·09	+0·065	+0·0064	+0·0099
	+ 5·07	+0·090	+0·0070	+0·0116		+ 5·13	+0·090	+0·0074	+0·0117
	+ 6·12	+0·120	+0·0074	+0·0142		+ 6·18	+0·121	+0·0077	+0·0146
	+ 7·16	+0·154	+0·0075	+0·0187		+ 7·22	+0·156	+0·0078	+0·0193
	+ 8·21	+0·190	+0·0073	+0·0245		+ 8·27	+0·193	+0·0074	+0·0251
	+ 9·27	+0·231	+0·0069	+0·0322		+ 9·32	+0·231	+0·0068	+0·0325
	+10·32	+0·273	+0·0062	+0·0417		+10·38	+0·277	+0·0055	+0·0428
	+11·37	+0·319	+0·0050	+0·0538		+11·43	+0·325	+0·0037	+0·0554
	+12·43	+0·366	+0·0037	+0·0683		+12·49	+0·374	+0·0014	+0·0707
	+13·49	+0·415	+0·0024	+0·0853		+13·54	+0·423	−0·0008	+0·0881
0·98	− 2·13	−0·113	+0·0100	+0·0190	1·02	− 2·18	−0·113	+0·0113	+0·0220
	− 1·15	−0·080	+0·0082	+0·0150		− 1·20	−0·079	+0·0089	+0·0180
	− 0·06	−0·045	+0·0068	+0·0121		− 0·11	−0·044	+0·0071	+0·0149
	+ 0·98	−0·013	+0·0054	+0·0100		+ 0·93	−0·011	+0·0051	+0·0131
	+ 2·01	+0·016	+0·0046	+0·0092		+ 1·96	+0·019	+0·0034	+0·0125
	+ 3·06	+0·049	+0·0045	+0·0093		+ 2·99	+0·047	+0·0028	+0·0122
	+ 4·10	+0·064	+0·0076	+0·0103		+ 5·08	+0·099	+0·0036	+0·0162
	+ 5·14	+0·090	+0·0082	+0·0122		+ 6·07	+0·132	+0·0032	+0·0191
	+ 6·19	+0·121	+0·0085	+0·0153		+ 7·16	+0·168	+0·0014	+0·0243
	+ 7·24	+0·157	+0·0077	+0·0201		+ 8·20	+0·209	−0·0012	+0·0314
	+ 8·28	+0·194	+0·0066	+0·0262		+10·29	+0·297	−0·0076	+0·0500
	+ 9·34	+0·238	+0·0053	+0·0345		+11·33	+0·345	−0·0117	+0·0635
	+10·38	+0·283	+0·0029	+0·0452		+12·37	+0·394	−0·0158	+0·0795
	+11·43	+0·331	−0·0005	+0·0580		+13·42	+0·437	−0·0186	+0·0959
	+12·48	+0·378	−0·0036	+0·0728					
	+13·53	+0·429	−0·0071	+0·0910					

19

TABLE 3—*continued*

Aerodynamic Coefficients of Model 6

M	$\alpha°$	C_L	C_m	C_D	M	$\alpha°$	C_L	C_m	C_D
1·42	− 1·97	−0·093	+0·0094	0·0198	1·61	− 1·77	−0·083	+0·0084	0·0179
	− 0·94	−0·062	+0·0069	0·0167		− 0·74	−0·053	+0·0061	0·0153
	+ 0·09	−0·031	+0·0046	0·0146		+ 0·29	−0·025	+0·0039	0·0136
	+ 1·12	−0·002	+0·0023	0·0136		+ 1·32	+0·004	+0·0017	0·0127
	+ 2·15	+0·026	+0·0002	0·0134		+ 2·35	+0·031	−0·0003	0·0128
	+ 3·18	+0·052	−0·0014	0·0141		+ 3·37	+0·056	−0·0020	0·0137
	+ 4·21	+0·077	−0·0025	0·0157		+ 4·40	+0·080	−0·0033	0·0154
	+ 5·24	+0·105	−0·0040	0·0179		+ 5·44	+0·107	−0·0049	0·0179
	+ 6·28	+0·134	−0·0056	0·0213		+ 6·47	+0·135	−0·0066	0·0214
	+ 7·32	+0·167	−0·0077	0·0258		+ 7·60	+0·165	−0·0087	0·0259
	+ 8·36	+0·205	−0·0104	0·0326		+ 8·54	+0·201	−0·0113	0·0327
	+ 9·40	+0·242	−0·0130	0·0406		+ 9·58	+0·234	−0·0137	0·0403
	+10·44	+0·281	−0·0160	0·0505		+10·62	+0·269	−0·0163	0·0498
	+11·48	+0·318	−0·0187	0·0617		+11·66	+0·304	−0·0188	0·0604
	+12·53	+0·356	−0·0212	0·0740		+12·70	+0·339	−0·0213	0·0727
	+13·57	+0·396	−0·0237	0·0894		+13·74	+0·374	−0·0239	0·0864
1·82	− 2·08	−0·082	+0·0073	0·0177	2·00	− 2·21	−0·080	+0·0073	0·0168
	− 1·05	−0·054	+0·0051	0·0149		− 1·18	−0·053	+0·0053	0·0141
	− 0·12	−0·027	+0·0030	0·0130		− 0·16	−0·027	+0·0032	0·0123
	+ 1·01	0·000	+0·0009	0·0120		+ 0·86	−0·002	+0·0013	0·0111
	+ 2·04	+0·026	−0·0010	0·0119		+ 1·88	+0·023	−0·0006	0·0106
	+ 3·06	+0·050	−0·0027	0·0124		+ 2·90	+0·047	−0·0023	0·0107
	+ 4·09	+0·073	−0·0040	0·0139		+ 3·93	+0·070	−0·0038	0·0120
	+ 5·12	+0·098	−0·0055	0·0162		+ 4·95	+0·092	−0·0050	0·0147
	+ 6·15	+0·125	−0·0072	0·0195		+ 5·97	+0·117	−0·0066	0·0180
	+ 7·18	+0·153	−0·0090	0·0235		+ 7·00	+0·144	−0·0083	0·0217
	+ 8·21	+0·183	−0·0112	0·0292		+ 8·03	+0·172	−0·0103	0·0267
	+ 9·20	+0·217	−0·0137	0·0364		+ 9·05	+0·200	−0·0125	0·0332
	+10·29	+0·249	−0·0159	0·0451		+10·08	+0·232	−0·0148	0·0416
	+11·32	+0·281	−0·0181	0·0547		+11·11	+0·261	−0·0168	0·0507
	+12·36	+0·313	−0·0203	0·0662		+12·14	+0·290	−0·0187	0·0607
	+13·40	+0·345	−0·0225	0·0784		+13·16	+0·319	−0·0206	0·0720

TABLE 4

Aerodynamic Coefficients of Model 7

M	$\alpha°$	C_L	C_m	C_D	M	$\alpha°$	C_L	C_m	C_D
0·40	− 2·13	−0·136	+0·0063	0·0219	0·70	− 2·17	−0·139	+0·0078	0·0225
	− 1·11	−0·104	+0·0060	0·0175		− 1·14	−0·108	+0·0073	0·0178
	− 0·09	−0·073	+0·0060	0·0139		− 0·10	−0·074	+0·0068	0·0142
	+ 0·93	−0·043	+0·0059	0·0113		+ 0·93	−0·043	+0·0064	0·0116
	+ 1·95	−0·014	+0·0058	0·0098		+ 1·96	−0·014	+0·0060	0·0100
	+ 2·97	+0·013	+0·0058	0·0091		+ 2·99	+0·014	+0·0060	0·0092
	+ 3·99	+0·038	+0·0063	0·0093		+ 4·02	+0·039	+0·0062	0·0094
	+ 5·01	+0·059	+0·0070	0·0106		+ 5·05	+0·062	+0·0073	0·0107
	+ 6·03	+0·083	+0·0084	0·0121		+ 6·09	+0·085	+0·0084	0·0122
	+ 7·05	+0·108	+0·0095	0·0143		+ 7·12	+0·112	+0·0095	0·0147
	+ 8·07	+0·137	+0·0106	0·0178		+ 8·16	+0·142	+0·0104	0·0186
	+ 9·10	+0·169	+0·0113	0·0226		+ 9·21	+0·176	+0·0111	0·0236
	+10·12	+0·202	+0·0121	0·0287		+10·25	+0·211	+0·0115	0·0302
	+11·15	+0·237	+0·0133	0·0362		+11·30	+0·249	+0·0121	0·0386
	+12·18	+0·275	+0·0141	0·0457		+12·35	+0·293	+0·0125	0·0497
	+13·22	+0·315	+0·0153	0·0570		+13·41	+0·340	+0·0129	0·0636
0·90	− 2·18	−0·146	+0·0108	0·0232	0·94	− 2·18	−0·148	+0·0118	0·0237
	− 1·14	−0·113	+0·0096	0·0181		− 1·14	−0·114	+0·0103	0·0184
	− 0·10	−0·077	+0·0084	0·0143		− 0·10	−0·079	+0·0090	0·0145
	+ 0·93	−0·044	+0·0074	0·0117		+ 0·94	−0·045	+0·0078	0·0116
	+ 1·97	−0·013	+0·0068	0·0098		+ 1·97	−0·014	+0·0070	0·0099
	+ 3·01	+0·016	+0·0063	0·0090		+ 3·01	+0·016	+0·0063	0·0091
	+ 4·05	+0·042	+0·0065	0·0090		+ 4·05	+0·043	+0·0066	0·0092
	+ 5·08	+0·064	+0·0079	0·0107		+ 5·09	+0·064	+0·0082	0·0109
	+ 6·13	+0·089	+0·0090	0·0125		+ 6·13	+0·090	+0·0093	0·0127
	+ 7·17	+0·117	+0·0097	0·0151		+ 7·18	+0·118	+0·0101	0·0154
	+ 8·22	+0·150	+0·0104	0·0191		+ 8·23	+0·153	+0·0105	0·0196
	+ 9·27	+0·187	+0·0105	0·0249		+ 9·28	+0·189	+0·0105	0·0254
	+10·32	+0·226	+0·0104	0·0324		+10·34	+0·233	+0·0099	0·0338
	+11·38	+0·272	+0·0099	0·0429		+11·40	+0·277	+0·0095	0·0438
	+12·44	+0·316	+0·0094	0·0547		+12·45	+0·321	+0·0084	0·0560
	+13·50	+0·364	+0·0086	0·0694		+13·51	+0·371	+0·0068	0·0711
0·98	− 2·17	−0·152	+0·0137	0·0242	1·02	− 2·16	−0·152	+0·0157	0·0265
	− 1·14	−0·116	+0·0114	0·0189		− 1·13	−0·117	+0·0133	0·0218
	− 0·10	−0·081	+0·0096	0·0147		− 0·09	−0·080	+0·0105	0·0169
	+ 0·94	−0·046	+0·0081	0·0120		+ 0·94	−0·046	+0·0088	0·0144
	+ 1·98	−0·014	+0·0070	0·0102		+ 1·98	−0·013	+0·0068	0·0126
	+ 3·02	+0·016	+0·0063	0·0094		+ 3·01	+0·018	+0·0053	0·0117
	+ 4·06	+0·043	+0·0066	0·0094		+ 4·05	+0·046	+0·0052	0·0119
	+ 5·10	+0·064	+0·0087	0·0111		+ 5·10	+0·067	+0·0074	0·0139
	+ 6·14	+0·089	+0·0097	0·0130		+ 6·14	+0·095	+0·0078	0·0157
	+ 7·19	+0·120	+0·0101	0·0159		+ 7·18	+0·126	+0·0073	0·0188
	+ 8·24	+0·153	+0·0103	0·0199		+ 8·23	+0·161	+0·0063	0·0235
	+ 9·29	+0·191	+0·0098	0·0260		+ 9·28	+0·200	+0·0052	0·0297
	+10·35	+0·236	+0·0085	0·0349		+10·33	+0·244	+0·0034	0·0385
	+11·40	+0·281	+0·0072	0·0451		+11·38	+0·292	+0·0004	0·0497
	+12·46	+0·329	+0·0050	0·0583		+12·42	+0·337	−0·0026	0·0625
	+13·51	+0·376	+0·0025	0·0729		+13·47	+0·390	−0·0077	0·0791

TABLE 4—*continued*

Aerodynamic Coefficients of Model 7

M	α°	C_L	C_m	C_D	M	α°	C_L	C_m	C_D
1·42	− 1·97	−0·129	+0·0166	0·0241	1·61	− 1·77	−0·113	+0·0145	0·0216
	− 0·94	−0·097	+0·0139	0·0198		− 0·79	−0·085	+0·0123	0·0180
	+ 0·04	−0·065	+0·0115	0·0167		+ 0·24	−0·056	+0·0101	0·0152
	+ 1·12	−0·035	+0·0091	0·0145		+ 1·27	−0·026	+0·0079	0·0134
	+ 2·15	−0·005	+0·0068	0·0133		+ 2·35	+0·002	+0·0058	0·0124
	+ 3·18	+0·023	+0·0047	0·0131		+ 3·38	+0·030	+0·0037	0·0124
	+ 4·21	+0·051	+0·0030	0·0137		+ 4·41	+0·055	+0·0021	0·0132
	+ 5·25	+0·076	+0·0020	0·0152		+ 5·44	+0·080	+0·0009	0·0155
	+ 6·28	+0·103	+0·0008	0·0177		+ 6·47	+0·106	−0·0004	0·0175
	+ 7·32	+0·133	−0·0005	0·0208		+ 7·51	+0·135	−0·0018	0·0210
	+ 8·36	+0·165	−0·0021	0·0255		+ 8·55	+0·165	−0·0036	0·0256
	+ 9·41	+0·205	−0·0046	0·0325		+ 9·59	+0·201	−0·0060	0·0323
	+10·45	+0·243	−0·0070	0·0408		+10·63	+0·237	−0·0083	0·0404
	+11·50	+0·282	−0·0097	0·0507		+11·67	+0·272	−0·0106	0·0500
	+12·54	+0·322	−0·0124	0·0626		+12·71	+0·307	−0·0131	0·0611
	+13·59	+0·361	−0·0149	0·0758		+13·75	+0·345	−0·0156	0·0743
1·82	− 1·91	−0·112	+0·0146	0·0211	2·00	− 2·20	−0·111	+0·0140	0·0210
	− 0·89	−0·083	+0·0124	0·0175		− 1·18	−0·085	+0·0120	0·0174
	+ 0·14	−0·056	+0·0102	0·0148		− 0·16	−0·059	+0·0100	0·0146
	+ 1·17	−0·028	+0·0080	0·0129		+ 0·87	−0·033	+0·0081	0·0126
	+ 2·20	−0·001	+0·0060	0·0118		+ 1·89	−0·006	+0·0062	0·0113
	+ 3·23	+0·025	+0·0040	0·0116		+ 2·91	+0·018	+0·0045	0·0112
	+ 4·25	+0·051	+0·0023	0·0123		+ 3·93	+0·043	+0·0028	0·0112
	+ 6·32	+0·099	−0·0002	0·0163		+ 4·96	+0·066	+0·0014	0·0124
	+ 7·35	+0·127	−0·0017	0·0197		+ 5·98	+0·089	+0·0004	0·0150
	+ 8·38	+0·155	−0·0033	0·0240		+ 7·01	+0·114	−0·0009	0·0180
	+ 9·42	+0·187	−0·0055	0·0298		+ 8·04	+0·141	−0·0024	0·0220
	+10·46	+0·223	−0·0080	0·0378		+ 9·06	+0·170	−0·0042	0·0271
	+11·50	+0·256	−0·0102	0·0468		+10·09	+0·200	−0·0061	0·0335
	+12·54	+0·289	−0·0123	0·0572		+11·13	+0·234	−0·0085	0·0420
	+13·58	+0·323	−0·0145	0·0692		+12·16	+0·264	−0·0105	0·0511
	+14·62	+0·355	−0·0167	0·0823		+13·19	+0·294	−0·0123	0·0619

TABLE 5

Aerodynamic Coefficients of Model 8

M	α°	C_L	C_m	C_D	M	α°	C_L	C_m	C_D
0·40	− 2·12	−0·149	+0·0089	+0·0234	0·70	− 2·21	−0·152	+0·0107	+0·0241
	− 0·08	−0·085	+0·0086	+0·0152		− 1·18	−0·121	+0·0103	+0·0197
	+ 0·94	−0·055	+0·0086	+0·0125		− 0·14	−0·089	+0·0097	+0·0156
	+ 1·96	−0·027	+0·0086	+0·0107		+ 0·89	−0·056	+0·0092	+0·0126
	+ 2·98	−0·001	+0·0086	+0·0098		+ 1·92	−0·027	+0·0091	+0·0105
	+ 4·00	+0·025	+0·0087	+0·0099		+ 2·95	0·000	+0·0089	+0·0097
	+ 5·02	+0·046	+0·0094	+0·0104		+ 3·98	+0·026	+0·0090	+0·0099
	+ 6·04	+0·071	+0·0112	+0·0122		+ 5·01	+0·049	+0·0099	+0·0101
	+ 7·06	+0·093	+0·0124	+0·0140		+ 6·05	+0·071	+0·0112	+0·0116
	+ 8·09	+0·124	+0·0137	+0·0173		+ 7·08	+0·097	+0·0125	+0·0139
	+ 9·11	+0·155	+0·0146	+0·0218		+ 8·12	+0·127	+0·0135	+0·0172
	+10·14	+0·191	+0·0155	+0·0279		+ 9·17	+0·163	+0·0144	+0·0226
	+11·17	+0·226	+0·0171	+0·0354		+10·22	+0·199	+0·0151	+0·0289
	+12·20	+0·264	+0·0181	+0·0449		+11·26	+0·236	+0·0161	+0·0368
	+13·23	+0·305	+0·0196	+0·0563		+12·31	+0·277	+0·0471	+0·0471
						+13·37	+0·321	+0·0177	+0·0598
0·90	− 2·22	−0·160	+0·0141	+0·0253	0·94	− 2·17	−0·164	+0·0155	+0·0256
	− 1·18	−0·128	+0·0130	+0·0202		− 1·13	−0·130	+0·0141	+0·0205
	− 0·14	−0·093	+0·0118	+0·0162		− 0·09	−0·095	+0·0126	+0·0164
	+ 0·90	−0·060	+0·0108	+0·0132		+ 0·95	−0·061	+0·0114	+0·0130
	+ 1·94	−0·028	+0·0103	+0·0108		+ 1·99	−0·030	+0·0107	+0·0108
	+ 2·97	+0·001	+0·0097	+0·0098		+ 3·02	0·000	+0·0099	+0·0100
	+ 4·01	+0·028	+0·0097	+0·0100		+ 4·06	+0·027	+0·0100	+0·0101
	+ 5·05	+0·050	+0·0109	+0·0106		+ 5·10	+0·049	+0·0115	+0·0107
	+ 6·09	+0·075	+0·0123	+0·0122		+ 6·15	+0·075	+0·0127	+0·0120
	+ 7·13	+0·103	+0·0132	+0·0146		+ 7·19	+0·104	+0·0138	+0·0151
	+ 8·18	+0·135	+0·0140	+0·0184		+ 8·24	+0·137	+0·0143	+0·0186
	+ 9·23	+0·172	+0·0142	+0·0236		+ 9·29	+0·174	+0·0143	+0·0240
	+10·29	+0·211	+0·0143	+0·0306		+10·35	+0·216	+0·0141	+0·0317
	+11·36	+0·260	+0·0138	+0·0412		+11·36	+0·257	+0·0143	+0·0410
	+12·41	+0·296	+0·0145	+0·0511		+12·47	+0·305	+0·0136	+0·0537
	+13·47	+0·343	+0·0146	+0·0652		+13·54	+0·349	+0·0132	+0·0670
0·98	− 2·16	−0·167	+0·0176	+0·0263	1·02	− 2·14	−0·167	+0·0199	+0·0296
	− 1·12	−0·133	+0·0157	+0·0211		− 1·16	−0·133	+0·0175	+0·0242
	− 0·08	−0·097	+0·0139	+0·0167		− 0·13	−0·097	+0·0151	+0·0192
	+ 0·95	−0·063	+0·0120	+0·0136		+ 0·91	−0·061	+0·0130	+0·0161
	+ 1·99	−0·030	+0·0110	+0·0116		+ 1·95	−0·029	+0·0114	+0·0137
	+ 3·03	−0·001	+0·0103	+0·0105		+ 2·98	+0·002	+0·0100	+0·0126
	+ 4·07	+0·028	+0·0103	+0·0101		+ 4·02	+0·031	+0·0093	+0·0126
	+ 5·11	+0·049	+0·0118	+0·0108		+ 5·06	+0·054	+0·0100	+0·0139
	+ 6·16	+0·075	+0·0136	+0·0124		+ 6·10	+0·081	+0·0108	+0·0155
	+ 7·21	+0·104	+0·0140	+0·0151		+ 7·15	+0·114	+0·0101	+0·0185
	+ 8·26	+0·138	+0·0143	+0·0190		+ 8·19	+0·148	+0·0097	+0·0227
	+ 9·31	+0·177	+0·0138	+0·0248		+ 9·24	+0·189	+0·0075	+0·0290
	+10·36	+0·219	+0·0130	+0·0324		+10·28	+0·233	+0·0050	+0·0376
	+11·37	+0·261	+0·0122	+0·0424		+11·34	+0·277	+0·0034	+0·0479
	+12·48	+0·309	+0·0108	+0·0548		+12·39	+0·321	+0·0018	+0·0597
	+13·54	+0·356	+0·0091	+0·0694		+13·45	+0·369	−0·0005	+0·0747

TABLE 5—continued

Aerodynamic Coefficients of Model 8

M	$\alpha°$	C_L	C_m	C_D	M	$\alpha°$	C_L	C_m	C_D
1·42	− 1·95	−0·141	+0·0208	0·0261	1·61	− 1·75	−0·125	+0·0188	0·0234
	− 0·92	−0·108	+0·0182	0·0216		− 0·72	−0·095	+0·0166	0·0196
	+ 0·11	−0·077	+0·0157	0·0180		+ 0·31	−0·066	+0·0144	0·0165
	+ 1·14	−0·046	+0·0132	0·0155		+ 1·34	−0·038	+0·0123	0·0144
	+ 2·17	−0·017	+0·0110	0·0140		+ 2·37	−0·009	+0·0102	0·0132
	+ 3·20	+0·012	+0·0088	0·0134		+ 3·40	+0·019	+0·0081	0·0129
	+ 4·23	+0·039	+0·0070	0·0138		+ 4·43	+0·044	+0·0065	0·0134
	+ 5·26	+0·064	+0·0062	0·0150		+ 5·46	+0·069	+0·0054	0·0149
	+ 6·30	+0·091	+0·0055	0·0171		+ 6·49	+0·095	+0·0044	0·0171
	+ 7·34	+0·121	+0·0044	0·0200		+ 7·53	+0·124	+0·0032	0·0203
	+ 8·39	+0·153	+0·0030	0·0242		+ 8·57	+0·154	+0·0016	0·0246
	+ 9·43	+0·189	+0·0010	0·0302		+ 9·61	+0·189	−0·0005	0·0307
	+10·48	+0·230	−0·0015	0·0378		+10·66	+0·226	−0·0027	0·0390
	+11·52	+0·269	−0·0039	0·0474		+11·70	+0·261	−0·0049	0·0475
	+12·57	+0·309	−0·0065	0·0587		+12·74	+0·298	−0·0073	0·0586
	+13·62	+0·349	−0·0090	0·0730		+13·79	+0·333	−0·0095	0·0720
1·82	− 1·90	−0·121	+0·0177	0·0226	2·00	− 2·19	−0·115	+0·0170	0·0220
	− 0·86	−0·093	+0·0155	0·0189		− 1·17	−0·088	+0·0149	0·0182
	+ 0·15	−0·065	+0·0134	0·0159		− 0·14	−0·061	+0·0129	0·0152
	+ 1·18	−0·038	+0·0114	0·0137		+ 0·88	−0·036	+0·0109	0·0129
	+ 2·21	−0·011	+0·0094	0·0125		+ 1·90	−0·010	+0·0091	0·0115
	+ 3·24	+0·015	+0·0074	0·0121		+ 2·93	+0·014	+0·0072	0·0107
	+ 4·27	+0·040	+0·0057	0·0125		+ 3·95	+0·039	+0·0054	0·0108
	+ 5·30	+0·064	+0·0045	0·0138		+ 4·97	+0·062	+0·0040	0·0121
	+ 6·33	+0·088	+0·0035	0·0161		+ 6·00	+0·085	+0·0032	0·0147
	+ 7·36	+0·115	+0·0024	0·0191		+ 7·02	+0·110	+0·0020	0·0176
	+ 8·40	+0·144	+0·0010	0·0231		+ 8·05	+0·137	+0·0006	0·0213
	+ 9·44	+0·175	−0·0009	0·0282		+ 9·08	+0·165	−0·0010	0·0263
	+10·48	+0·210	−0·0032	0·0359		+10·11	+0·195	−0·0029	0·0320
	+11·52	+0·242	−0·0051	0·0446		+11·14	+0·226	−0·0049	0·0396
	+12·56	+0·275	−0·0072	0·0544		+12·17	+0·258	−0·0070	0·0483
	+13·60	+0·308	−0·0092	0·0656		+13·20	+0·288	−0·0088	0·0592

EQUATION OF LEADING EDGE $\quad \frac{y}{C_0} = 0.25 \left(\frac{x}{C_0}\right) \left\{1.25 - 0.25\left(\frac{x}{C_0}\right)^4\right\}$

EQUATION OF CENTRE SECTION $\quad \frac{z}{C_0} = 0.64141 \left(\frac{x}{C_0}\right)\left(1 - \frac{x}{C_0}\right) \Big/ \left\{5 - \left(\frac{x}{C_0}\right)^4\right\}$

EQUATION OF SHOULDER $\quad y = 0.75 \frac{x}{C_0} (y) \; l.e.$

72.6°

'SHOULDER' LINE
WINGS 6, 7 AND 8

⊕ MOMENT CENTRE
(58.4% C_0)

$0.694 C_0$

"$\overline{C}$"

MODEL SUPPORT
AND BALANCE
SHIELD

C_0

S_T

PLANFORM AND TYPICAL CROSS-SECTIONS.   CENTRE SECTION.
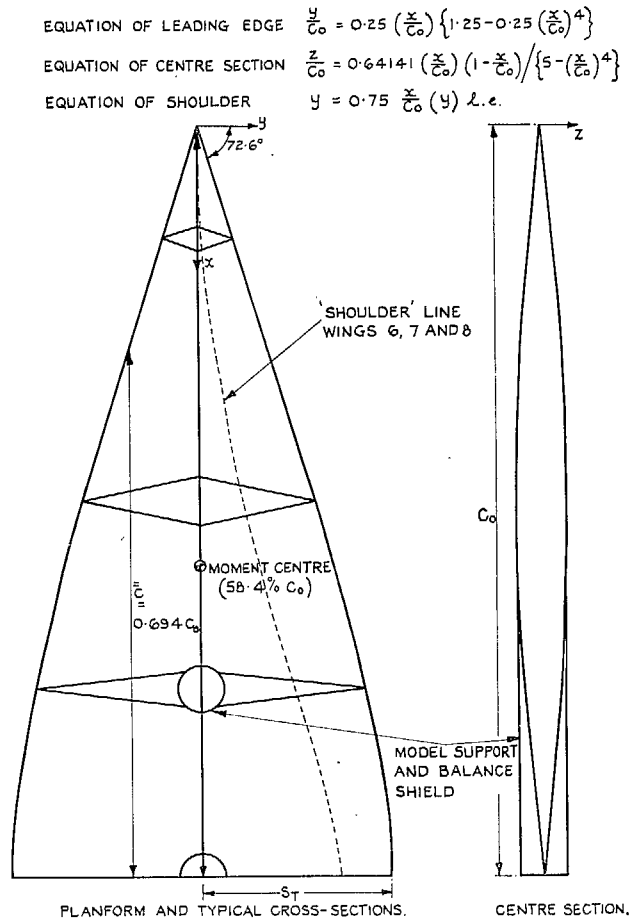
FIG. 1.   Details of wing 5 and basic planform.

WING 8
WING 7
WING 6

$\frac{z}{C_0}$ 0.05

0.10

$\frac{x}{C_0}$

NOTES. (i) CROSS-SECTIONS OF WING 8
ARE APPROXIMATELY THE SAME
AS THOSE OF WING 7.
(ii) THE CROSS-SECTION SHAPES
ARE DISPLACED RELATIVE TO
EACH OTHER BY THE CHORDWISE
CAMBER ILLUSTRATED ABOVE.
(SEE ALSO FIG. 3)

₵
WING 5
WING 6
WING 7

$\frac{x}{C_0} = 0.181$

WING 5
WING 6
WING 7

$\frac{x}{C_0} = 0.409$

WING 5
WING 6
WING 7

$\frac{x}{C_0} = 0.590$

WING 5

WING 7
(WING 6 APPROXIMATELY
SAME SHAPE)

$\frac{x}{C_0} = 0.810$

TRAILING EDGE (ALL WINGS)

FIG. 2.   Cross-sections: wings 5, 6, 7 and 8.

∝m INCIDENCE OF THE PLANE CONTAINING THE
WING APEX AND TRAILING EDGE AT
THE DESIGN LIFT.

WING 6, ∝m = 3·09°

WING 7, ∝m = 4·74°

WING 8, ∝m = 4·97°
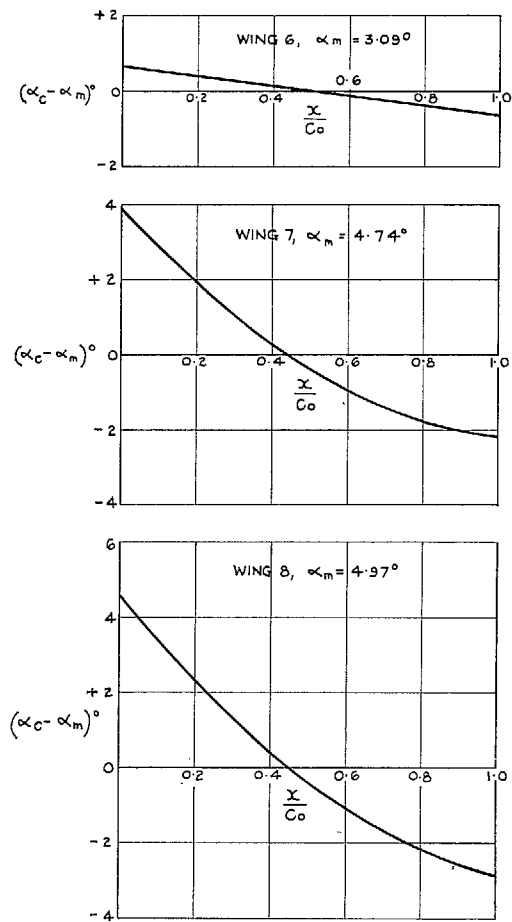
FIG. 3. Variation of centre-line incidence of the cambered wings at design lift.

CENTRE SECTION
LEADING EDGE
STING SHIELD
WING 6
0·00273C₀
(0·060")
TRAILING EDGE

CENTRE SECTION
LEADING EDGE
STING SHIELD
WING 7
0·01364C₀
(0·300")
TRAILING EDGE

CENTRE SECTION
LEADING EDGE
STING SHIELD
WING 8
0·01364C₀
(0·300")
TRAILING EDGE
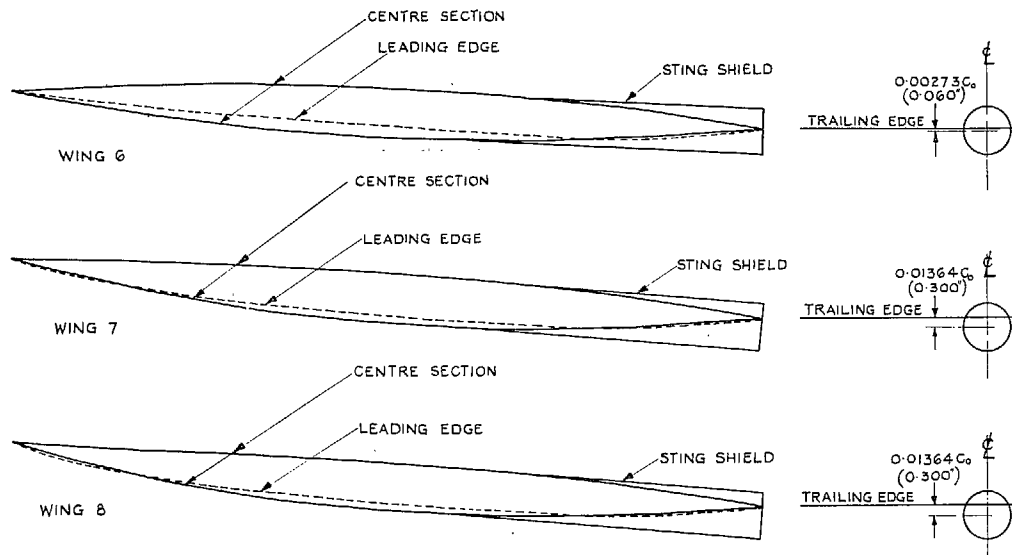
FIG. 4. Details of sting shields: models 6, 7 and 8.

$\frac{L(x)}{S_T}$

WING 7, $C_L = 0·05, M = 1·0$
WING 8, $C_L = 0·05, M = 1·89$
WING 5 $C_L = 0·05, M = 1·0$
WING 6 $C_L = 0·05, M = 1·0$

x/c_0
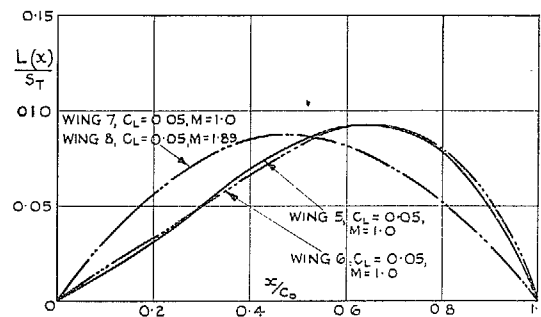
FIG. 5. Chordwise variation of cross-load: wings 5, 6, 7 and 8.
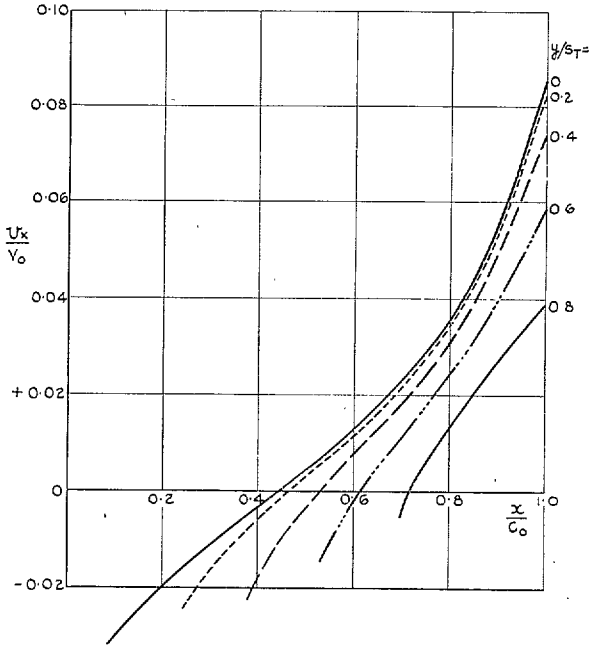
FIG. 6. Velocity distributions on wing 5 at
zero lift.
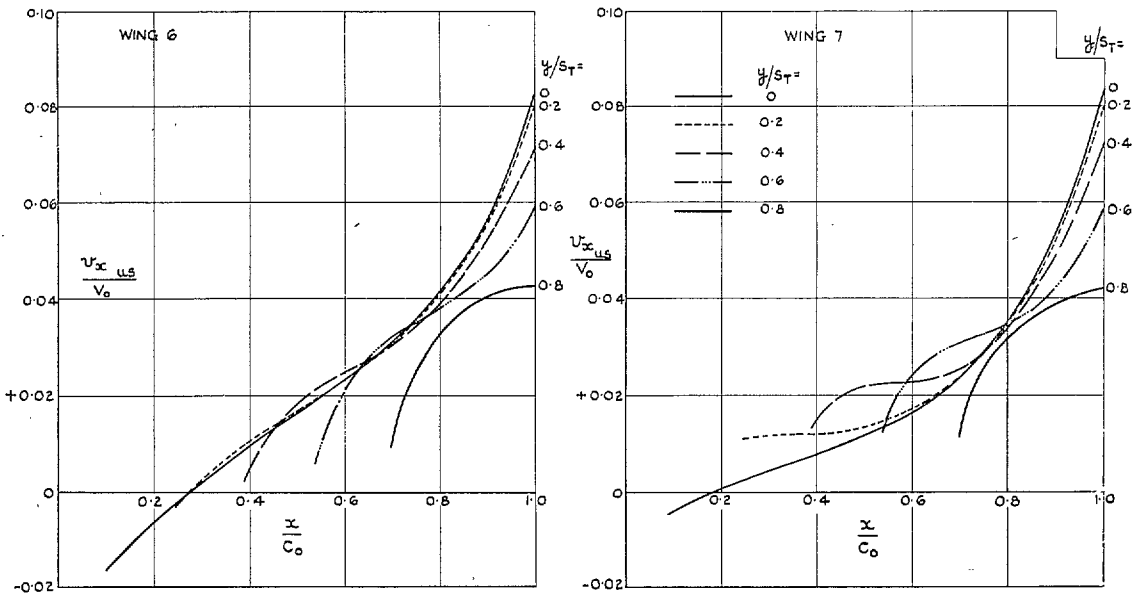
FIG. 7. Velocity distributions on wings 6 and 7 at the design lift.

27
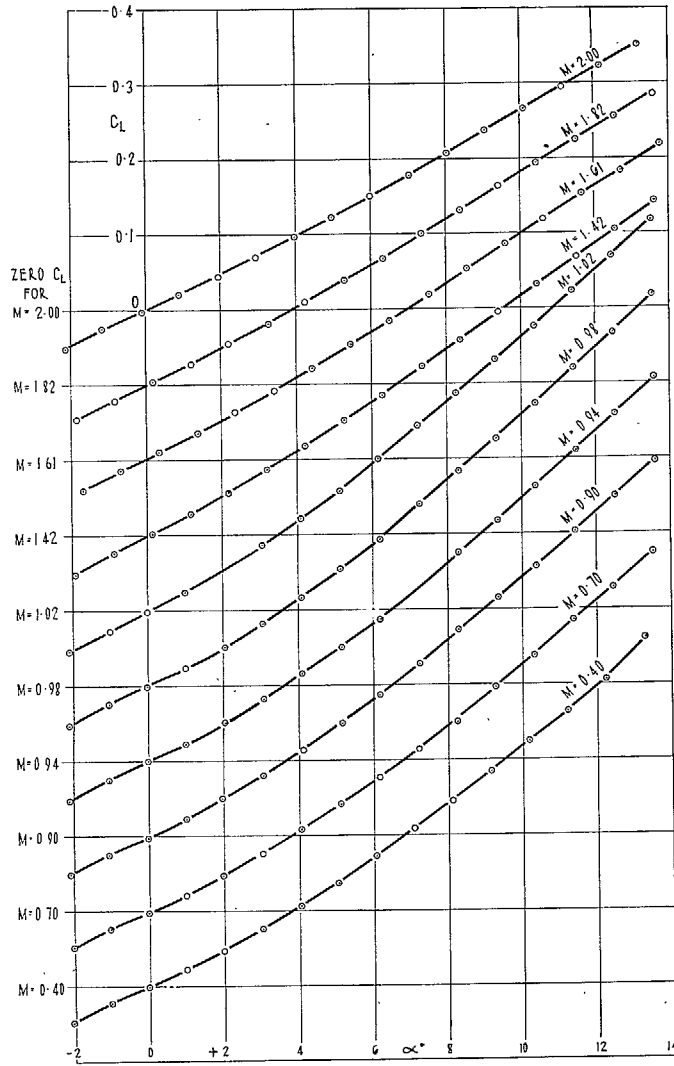
FIG. 8.   Variation of C_L with α: model 5.
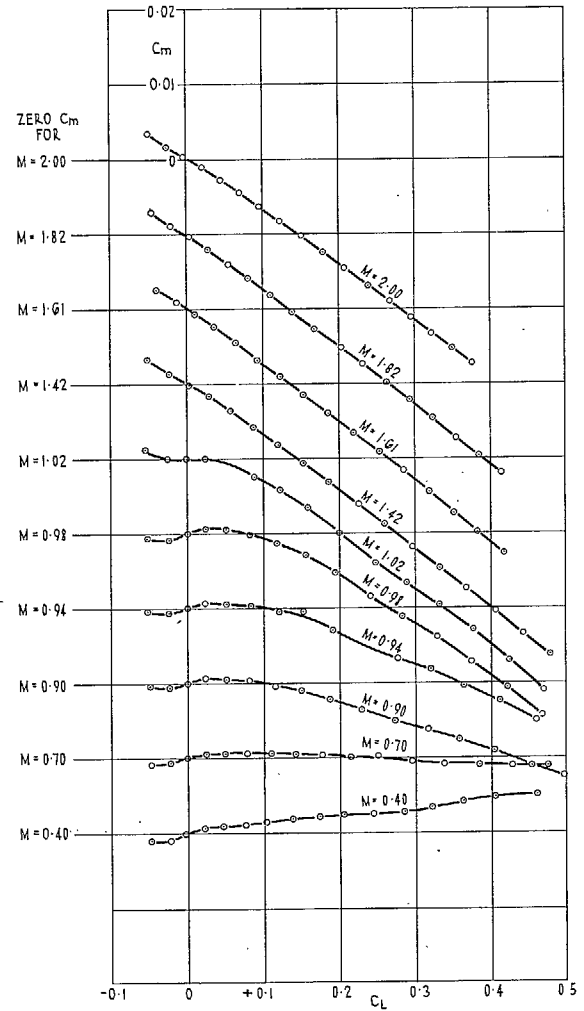
FIG. 9.   Variation of C_m with C_L: model 5.
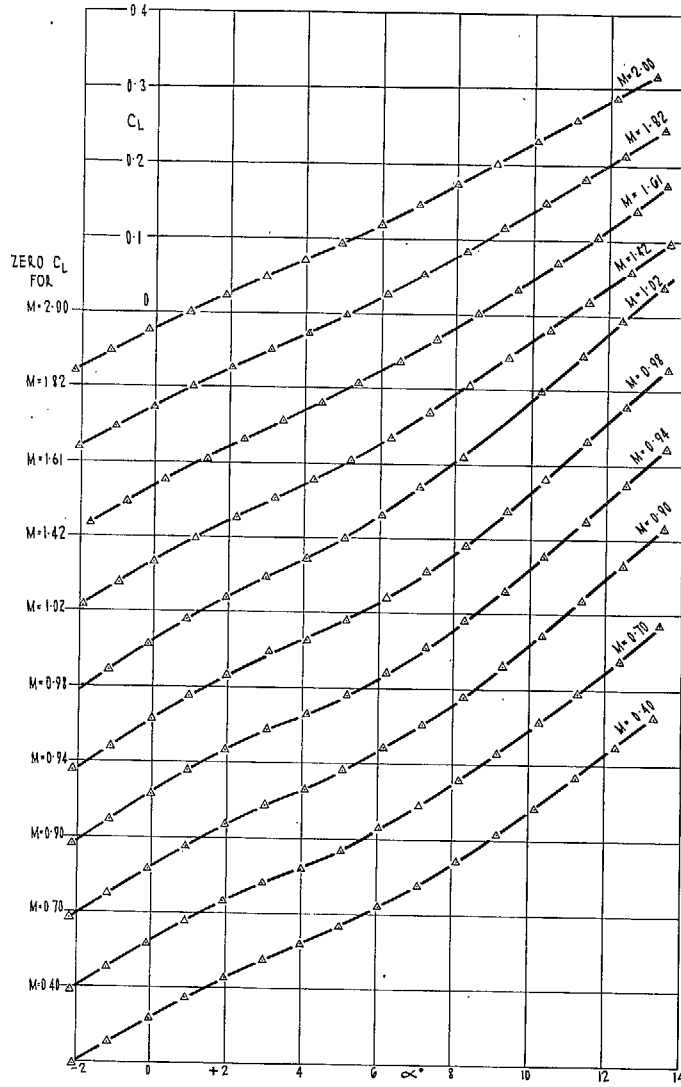
FIG. 10.   Variation of C_L with α: model 6.
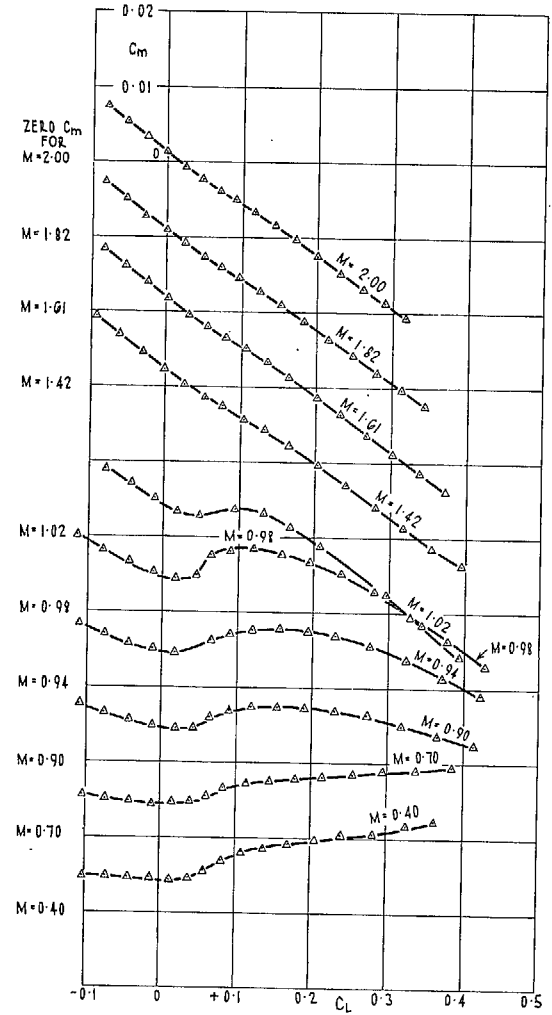
FIG. 11.   Variation of C_m with C_L: model 6.
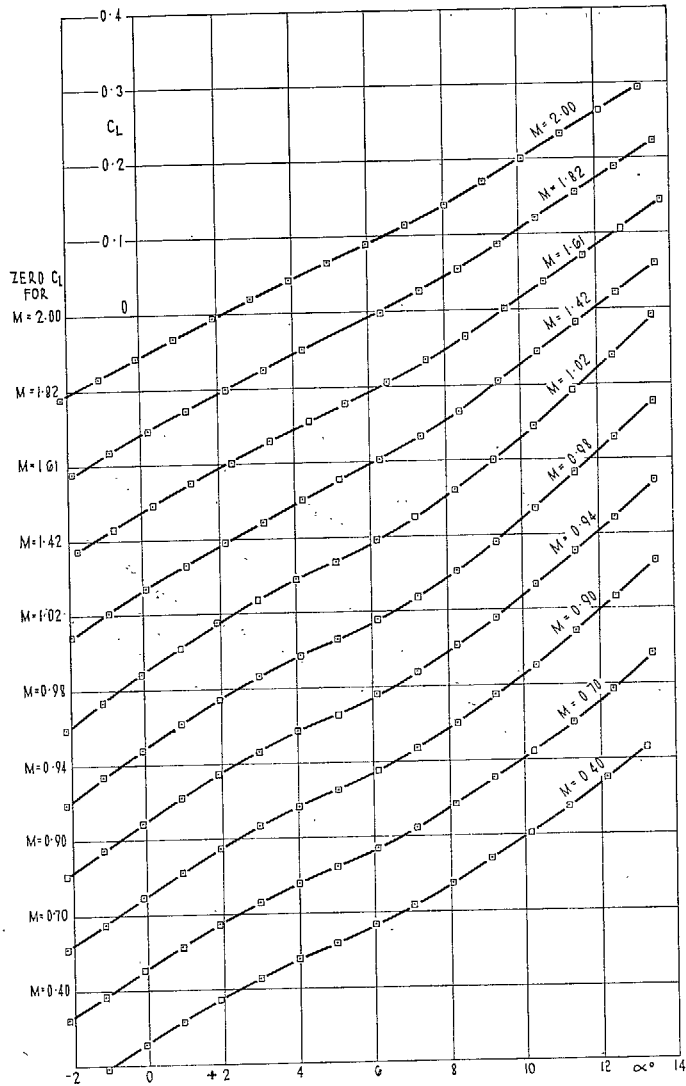
FIG. 12.   Variation of C_L with α: model 7.
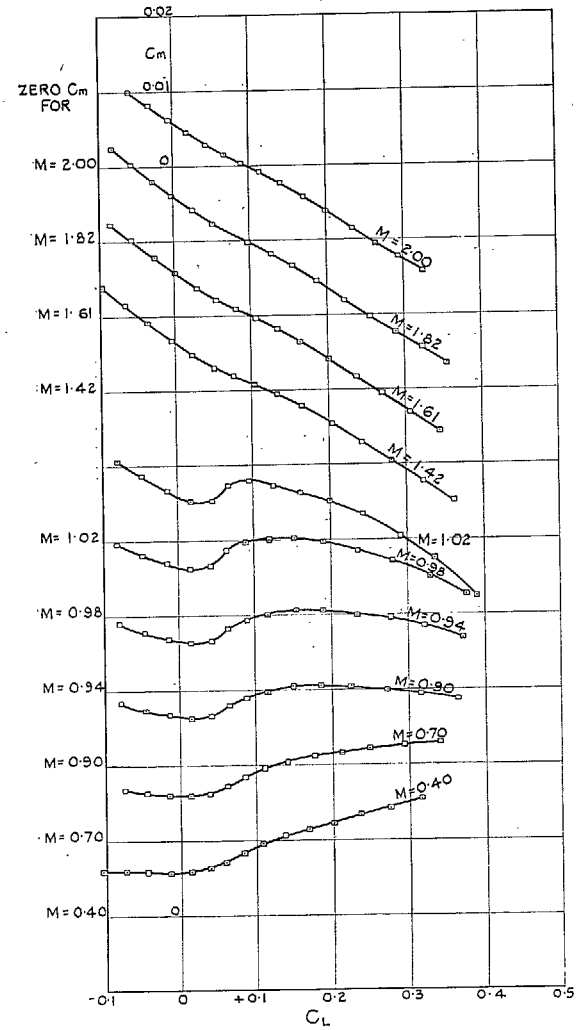
FIG. 13.   Variation of C_m with C_L: model 7.
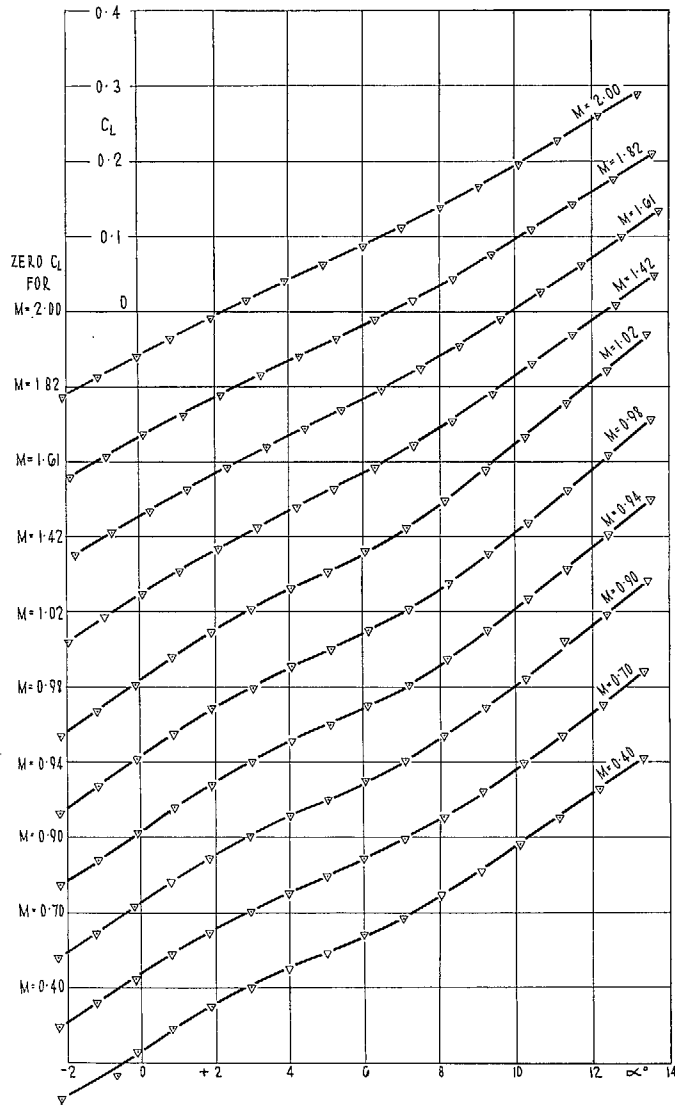
Fig. 14. Variation of C_L with α: model 8.
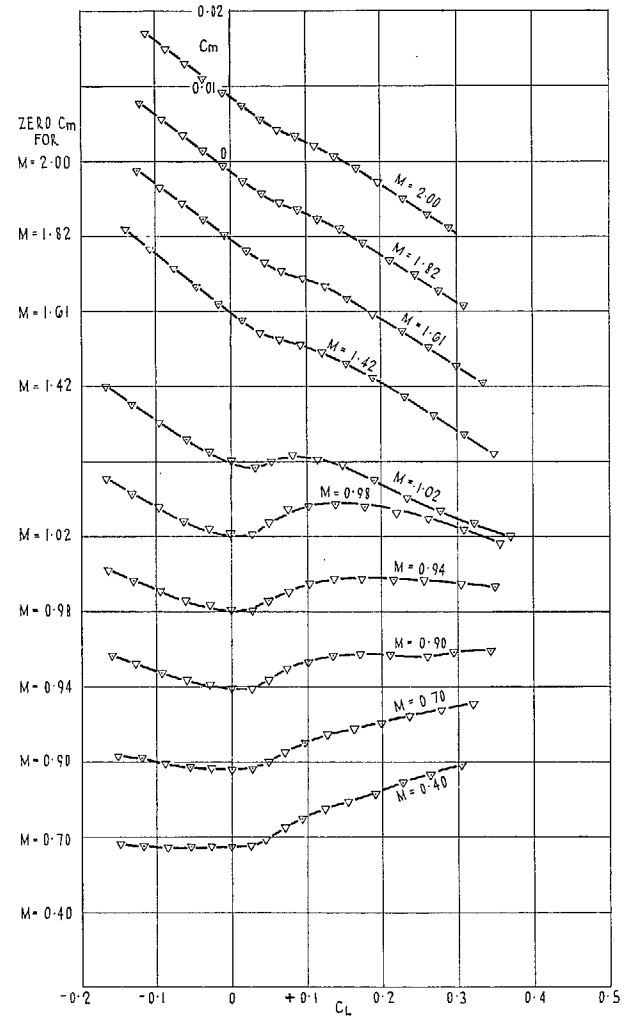
Fig. 15. Variation of C_m with C_L: model 8.
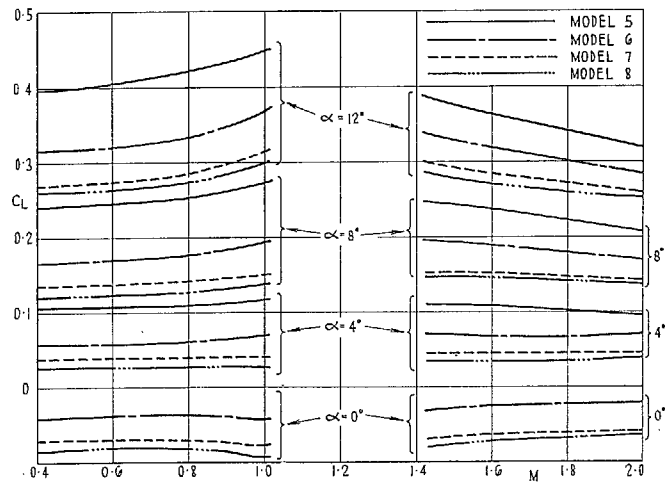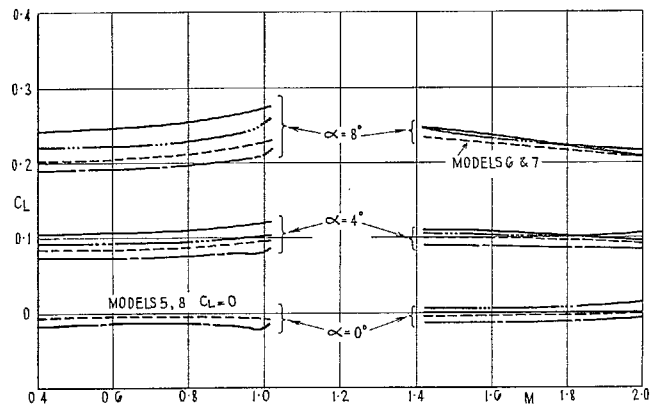
FIG. 16a and b.   Variation of C_L with Mach number.
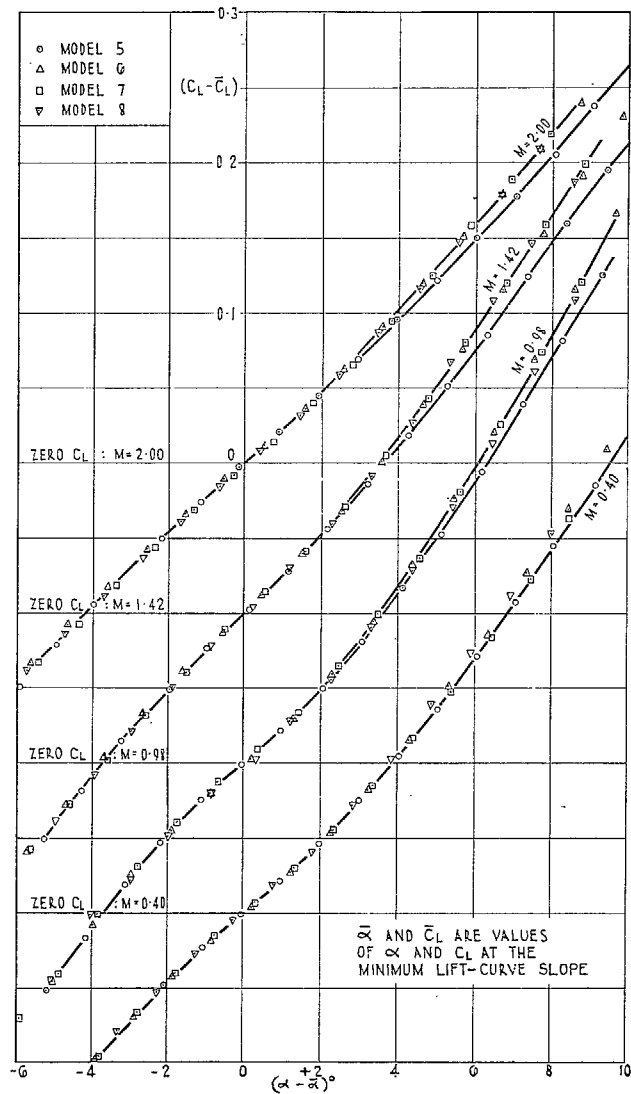
FIG. 17.   Variation of $(C_L - \overline{C}_L)$ with $(\alpha - \overline{\alpha})°$.

33
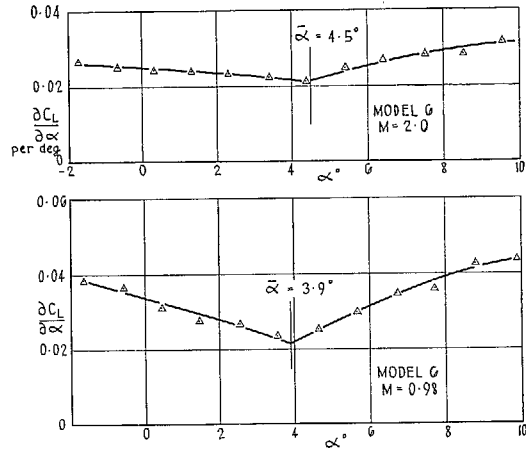
Fig. 18. Typical variations of $\partial C_L/\partial\alpha$ with α.
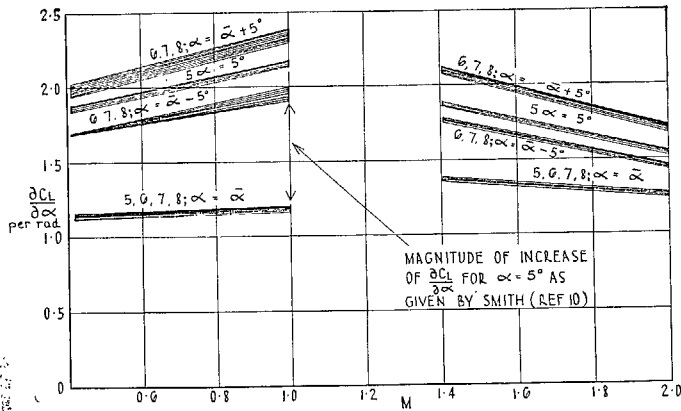
Fig. 20. Variation of $\bar{\alpha}$ with Mach number.

Fig. 21. Variation of $\overline{C}_L$ with Mach number.
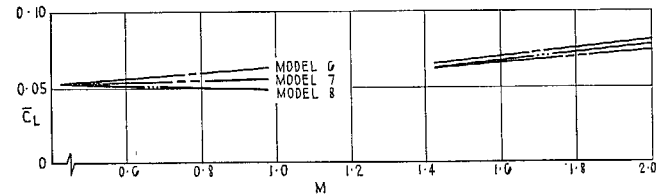
Fig. 19. Variation of $\partial C_L/\partial\alpha$ with Mach number.
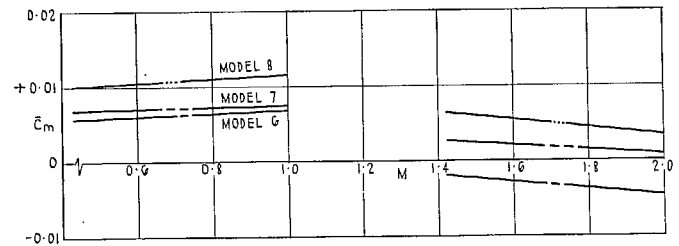
Fig. 22. Variation of $\overline{C}_m$ with Mach number.
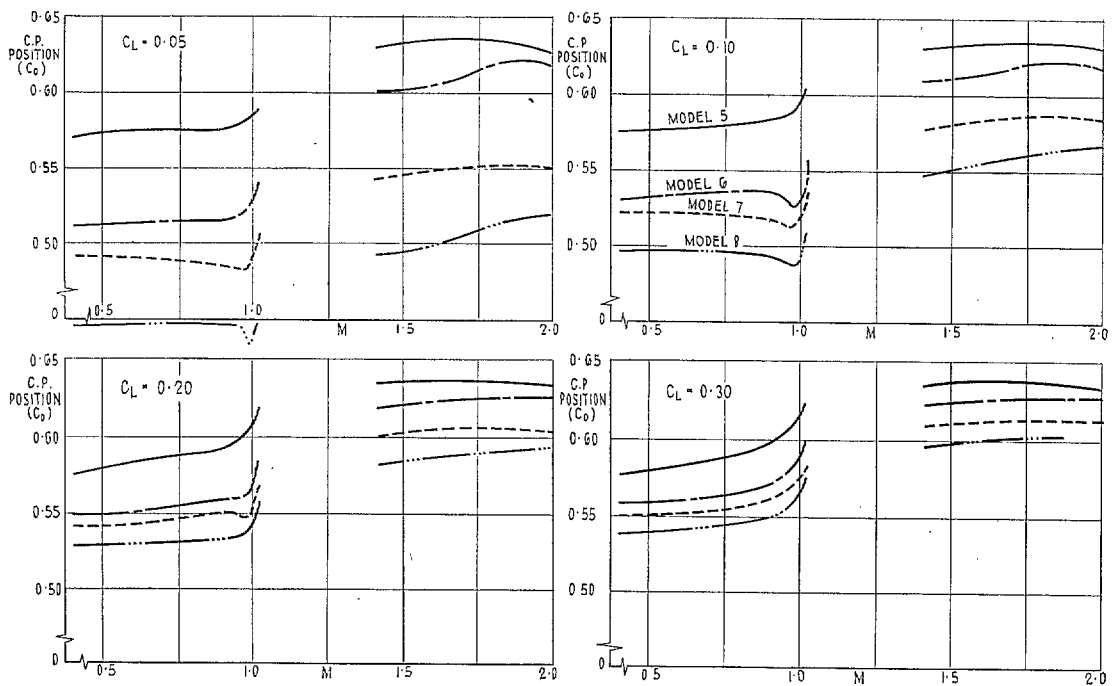
FIG. 23. Position of centre of pressure on root chord: variation with Mach number at constant C_L.
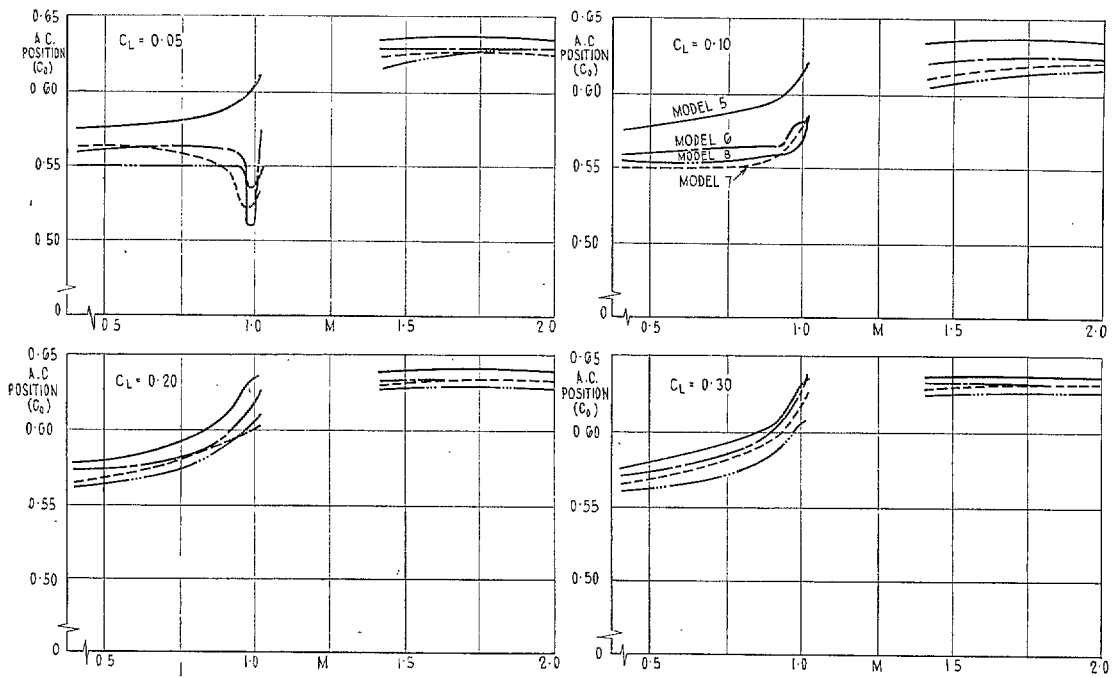
FIG. 24. Position of aerodynamic centre on root chord: variation with Mach number at constant C_L.

34
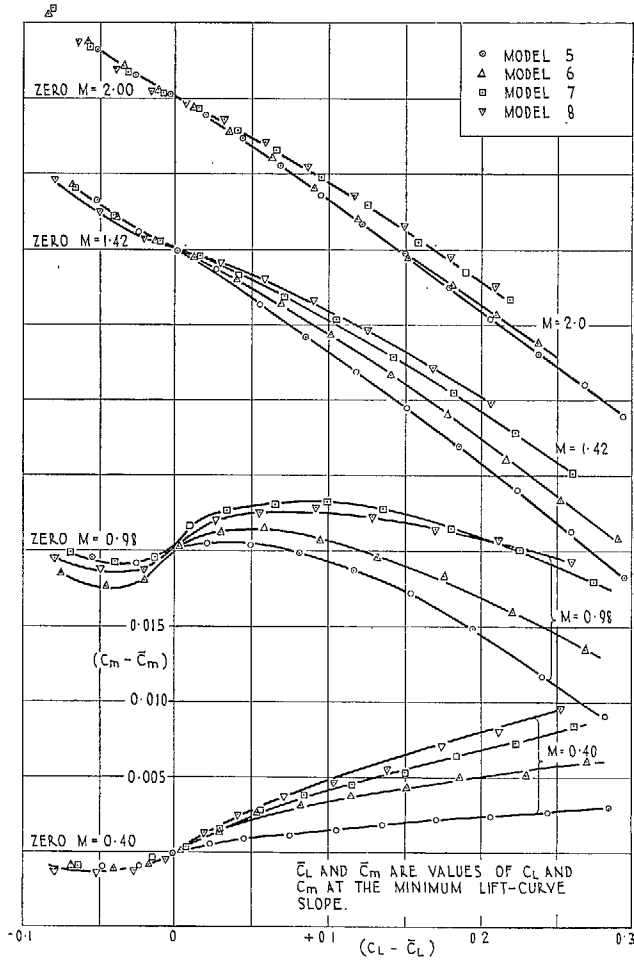
FIG. 25. Variation of $(C_m - \overline{C}_m)$ with $(C_L - \overline{C}_L)$.

FIG. 26. Comparison of experimental and theoretical centre-of-pressure positions.
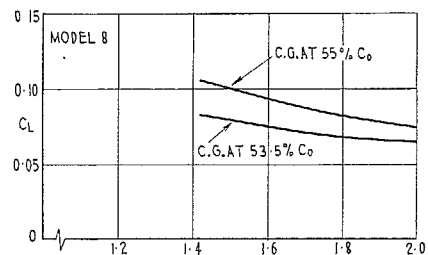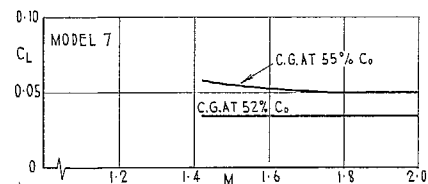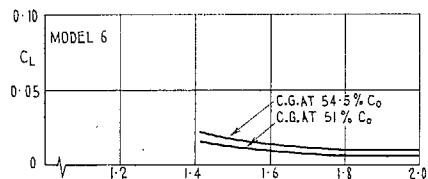
N.B.
VALUES PLOTTED ARE BASED ON UNCORRECTED
VALUES OF C_m. THE EFFECT OF THE CORRECTION
IS NEGLIGIBLE FOR WING 6, AND INCREASES (C_L)
TRIM FOR WINGS 7 AND 8 BY ABOUT 0·01.

FIG. 27.   Variation of trim C_L with
Mach number.
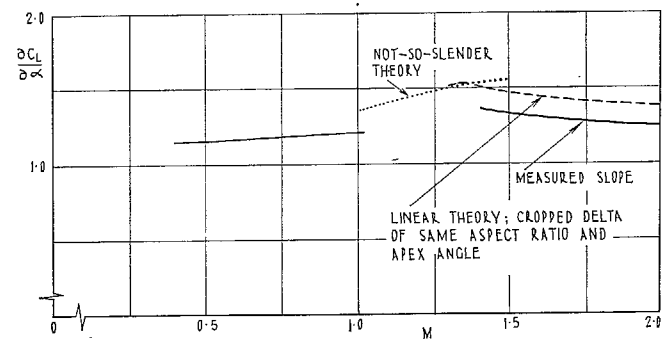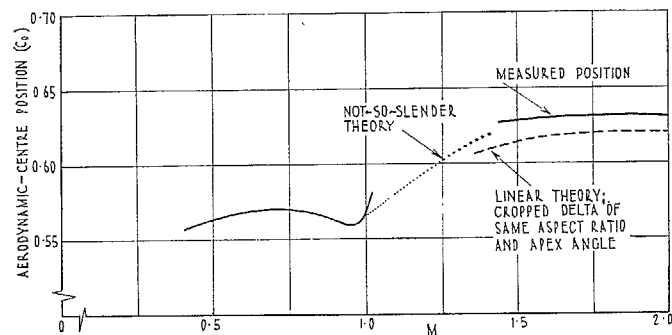
FIG. 28.   Comparison of aerodynamic-centre position
and lift-curve slope with theory: wing 5, $\alpha = 0$.
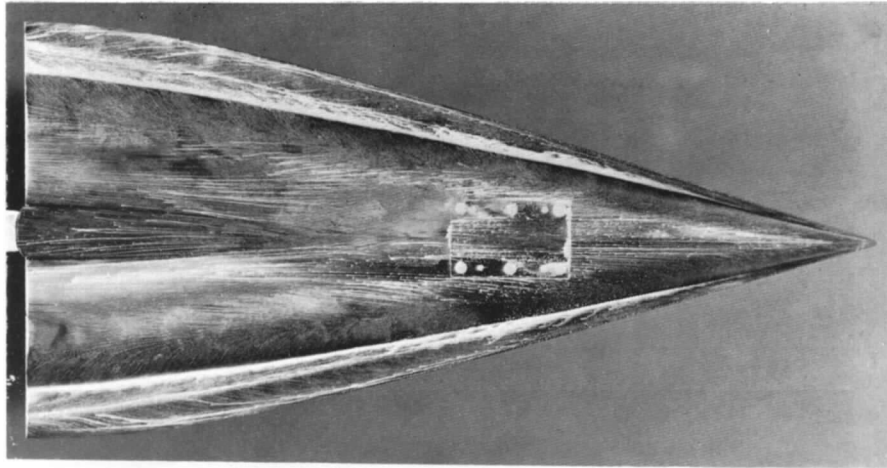
$\alpha = 8 \cdot 6^\circ, \qquad C_L = 0 \cdot 252$
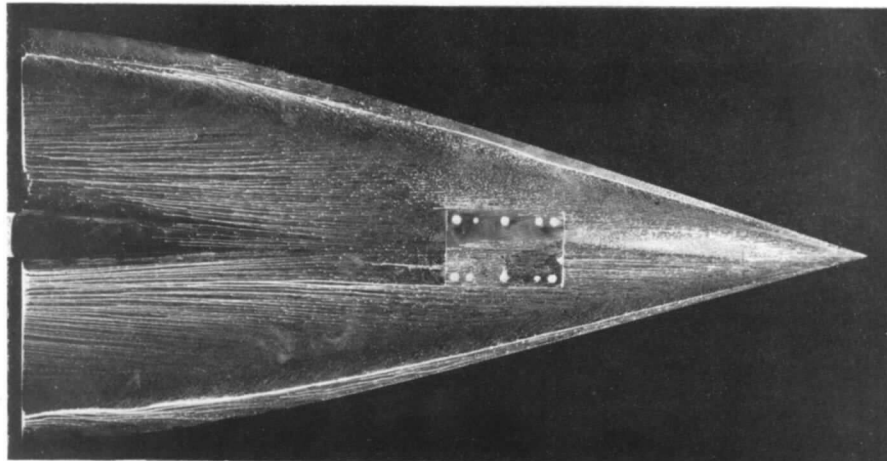
$\alpha = 5 \cdot 8^\circ, \qquad C_L = 0 \cdot 161$
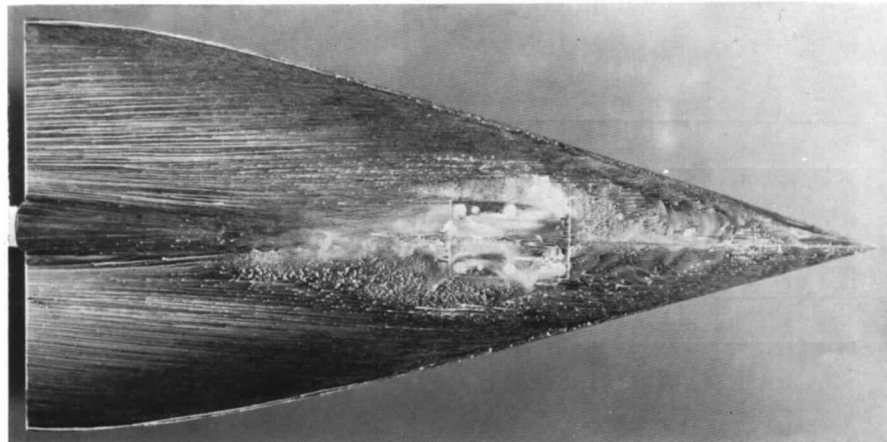
$\alpha = 1 \cdot 3^\circ, \qquad C_L = 0 \cdot 035$

FIG. 29.   Oil flow on upper surface of wing 5 at $M = 1 \cdot 61$.

37
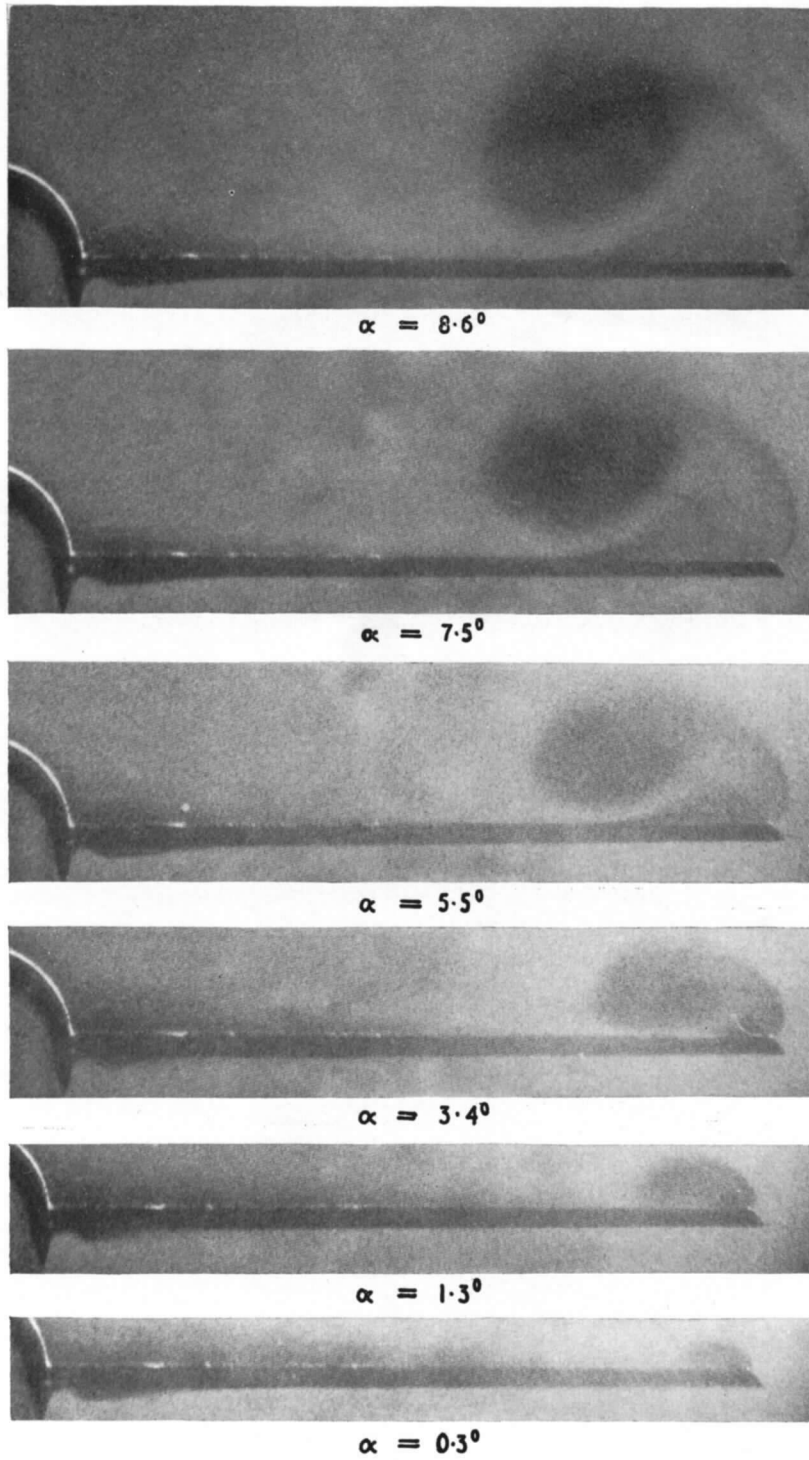
FIG. 30. Vapour screen over wing 5 at $M = 1 \cdot 6$: $0 \cdot 5$ in. ahead of trailing edge.

$\alpha = 10 \cdot 63^0, \quad \alpha - \bar{\alpha} = 5 \cdot 78^0, \quad C_L = 0 \cdot 237$
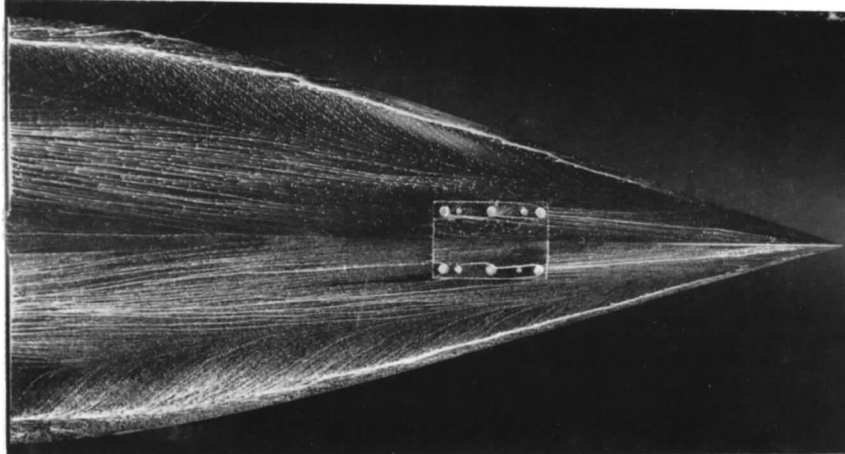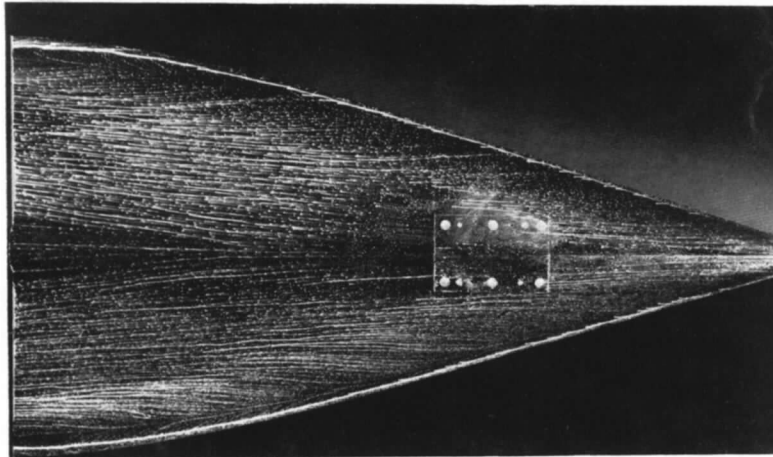
$\alpha = 7 \cdot 51^0, \quad \alpha - \bar{\alpha} = 2 \cdot 66^0, \quad C_L = 0 \cdot 135$
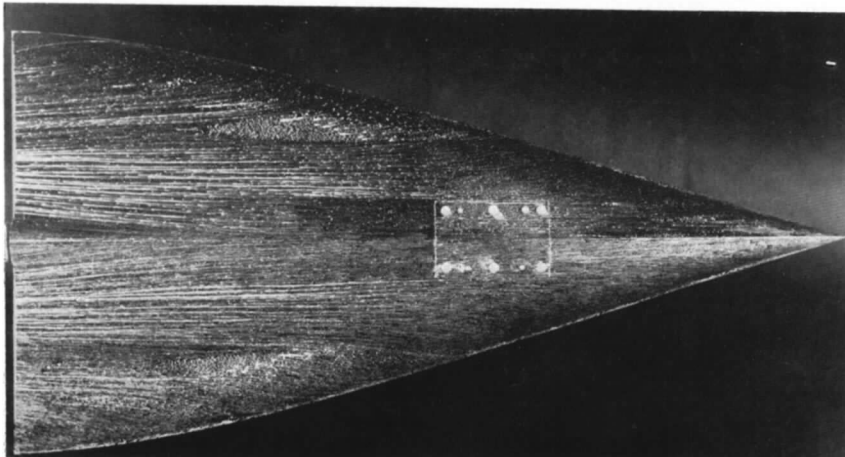
$\alpha = 5 \cdot 44, \quad \alpha - \bar{\alpha} = 0 \cdot 59, \quad C_L = 0 \cdot 080$

FIG. 31.   Oil flow on upper surface of wing 7 at $M = 1 \cdot 61$.

$\alpha = 10{\cdot}63, \quad \alpha - \bar{\alpha} = 5{\cdot}78$

$\alpha = 9{\cdot}59, \quad \alpha - \bar{\alpha} = 4{\cdot}74$

$\alpha = 8{\cdot}55, \quad \alpha - \bar{\alpha} = 3{\cdot}70$

$\alpha = 7{\cdot}51, \quad \alpha - \bar{\alpha} = 2{\cdot}66$

$\alpha = 6{\cdot}47, \quad \alpha - \bar{\alpha} = 1{\cdot}62$

$\alpha = 5{\cdot}44, \quad \alpha - \bar{\alpha} = 0{\cdot}59$
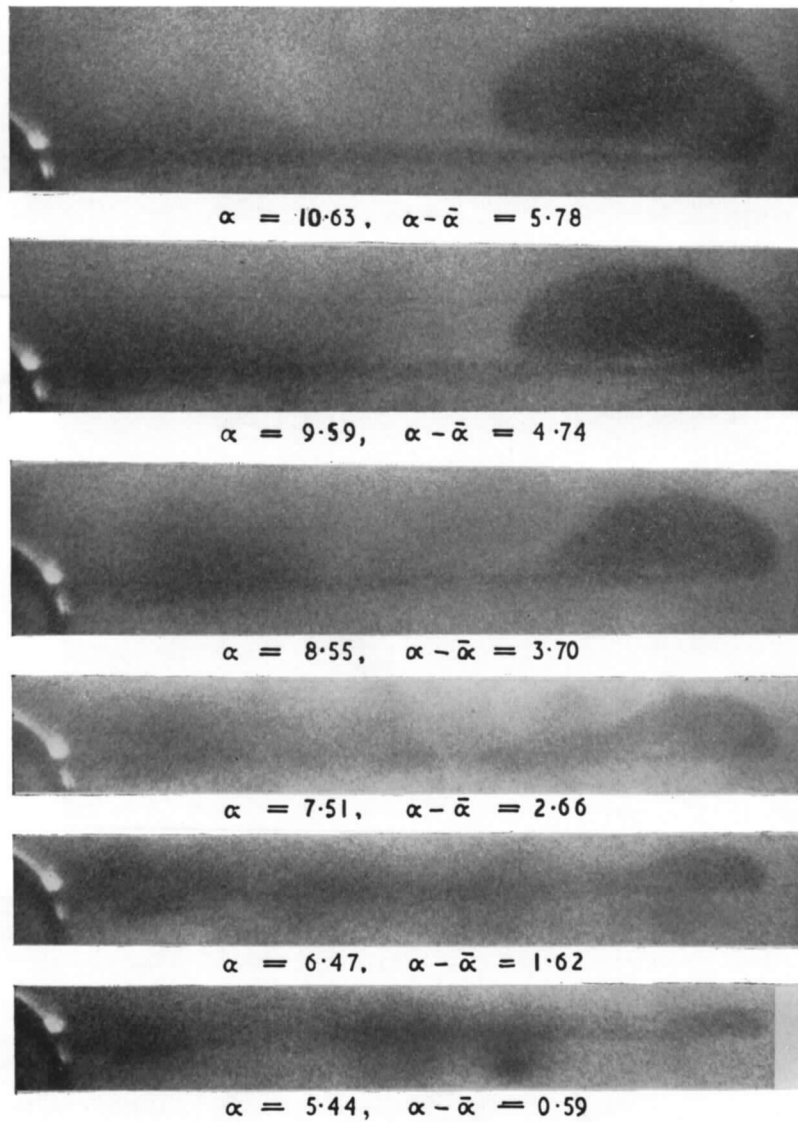
FIG. 32. Vapour screen over wing 7 at $M = 1{\cdot}6$: $0{\cdot}5$ in. ahead of trailing edge.

$\alpha = 10 \cdot 09^0, \quad \alpha - \bar{\alpha} = 4 \cdot 89^0, \quad C_L = 0 \cdot 200$
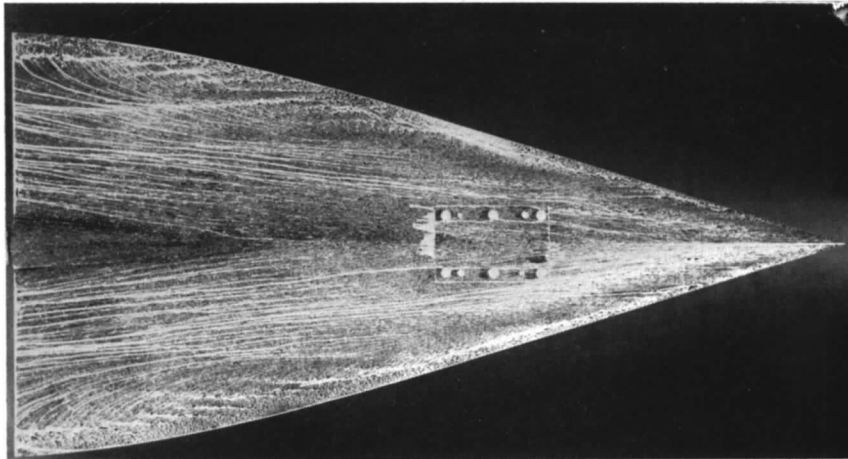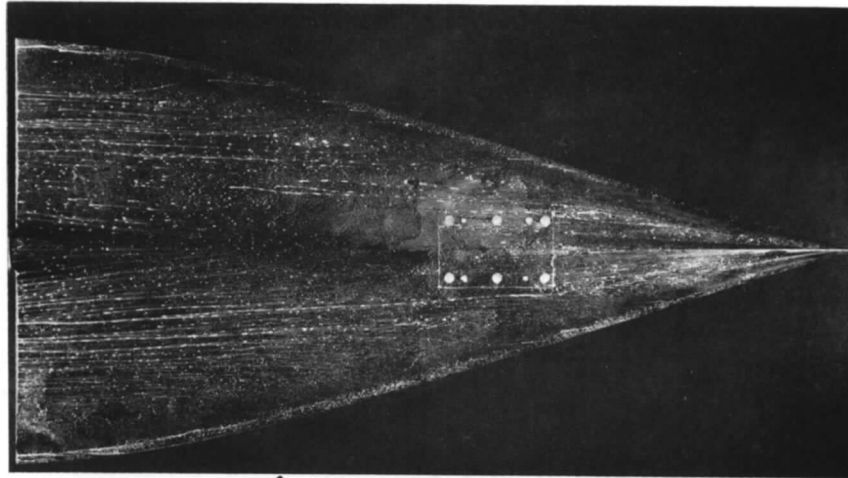
$\alpha = 7 \cdot 01^0, \quad \alpha - \bar{\alpha} = 1 \cdot 81, \quad C_L = 0 \cdot 114$
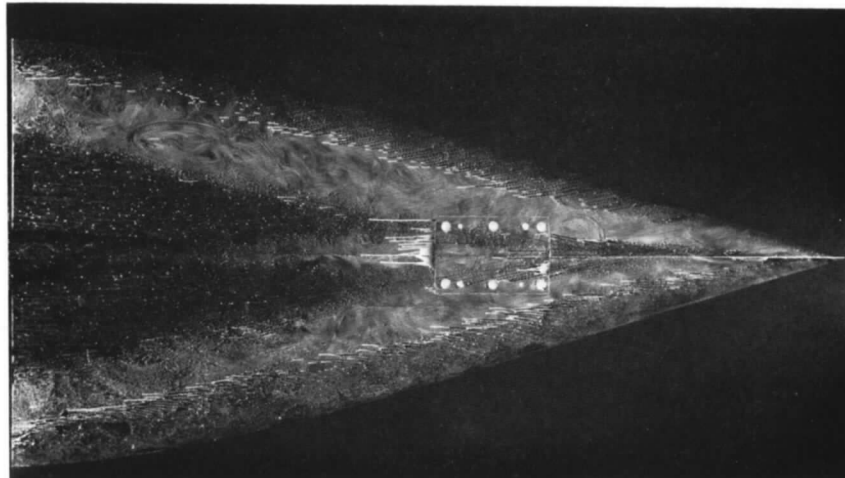
$\alpha = 4 \cdot 96^0, \quad \alpha - \bar{\alpha} = 0 \cdot 24, \quad C_L = 0 \cdot 089$

FIG. 33. Oil flow on upper surface of wing 7 at $M = 2 \cdot 0$.

41
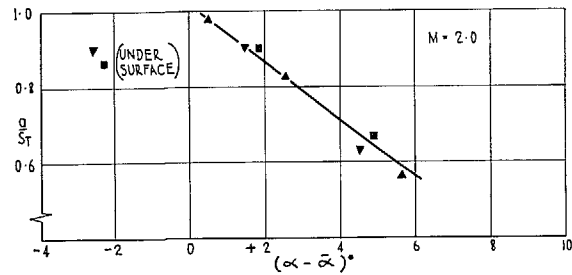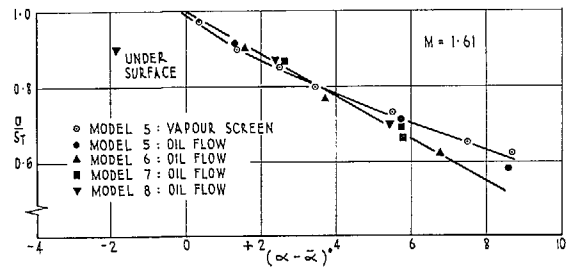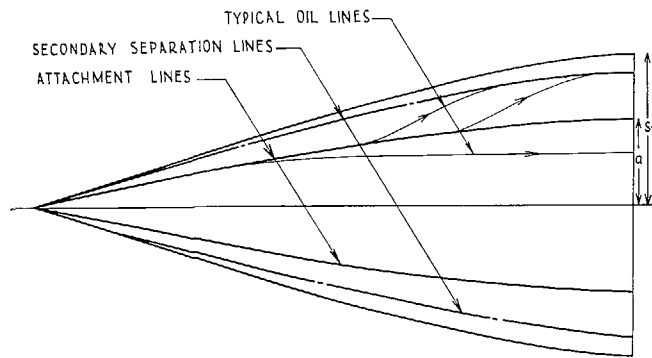
FIG. 34. Variation of attachment-line position with $(\alpha - \bar{\alpha})$.
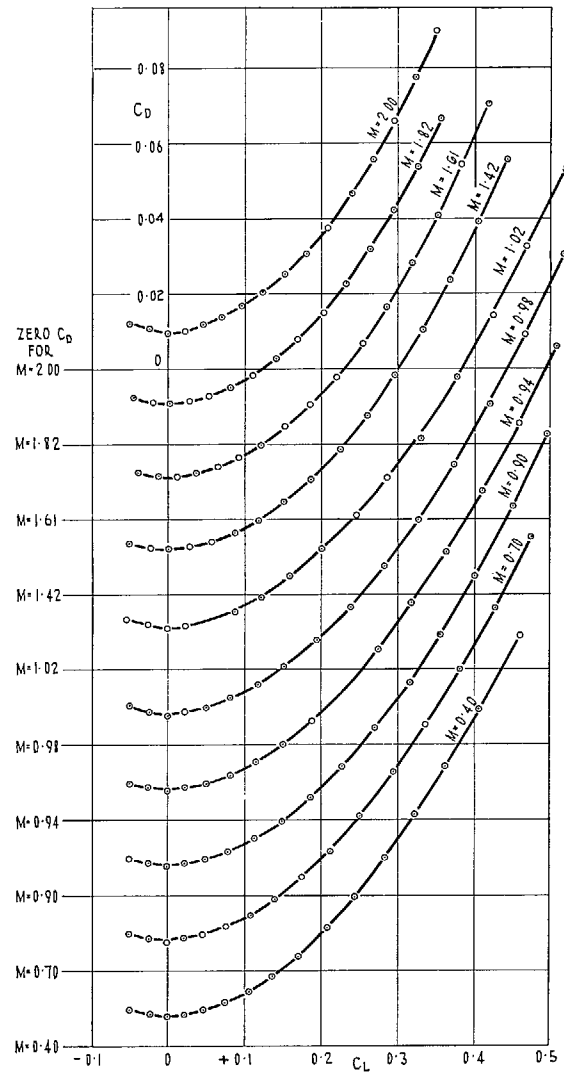
FIG. 35. Variation of C_D with C_L: model 5.

42
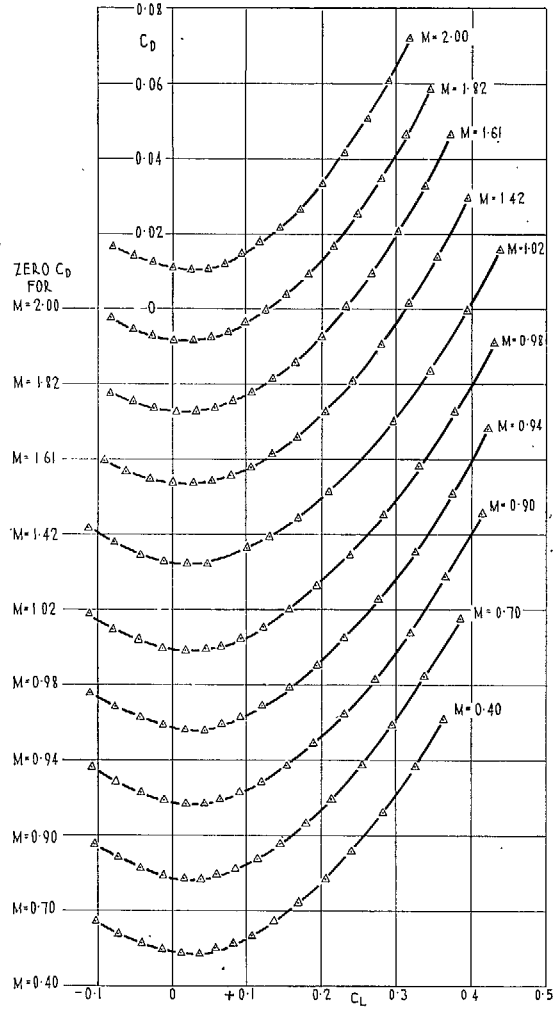
FIG. 36. Variation of C_D with C_L: model 6.
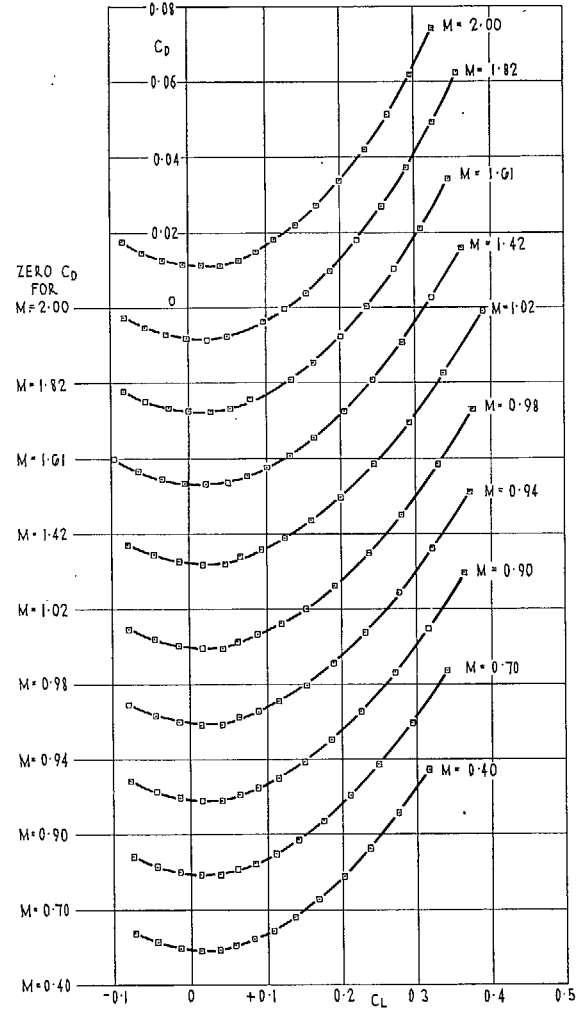
FIG. 37. Variation of C_D with C_L: model 7.
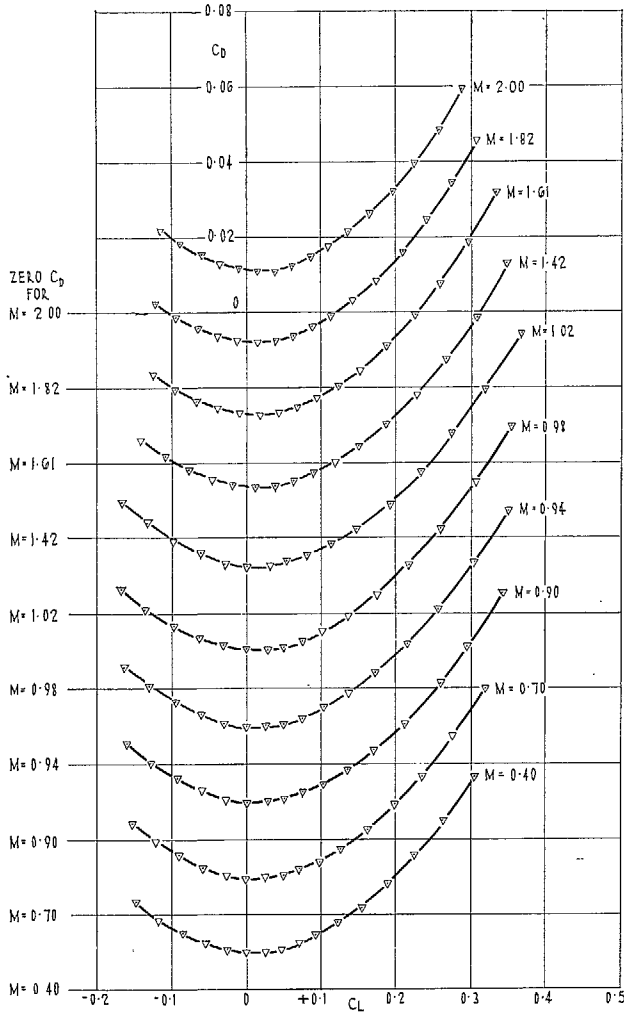
FIG. 38. · Variation of C_D with C_L: model 8.
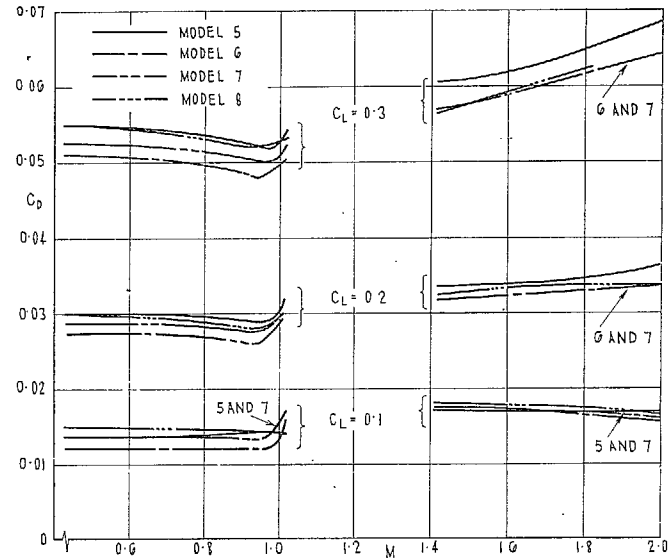
FIG. 39. Variation of C_D at fixed C_L with Mach number.
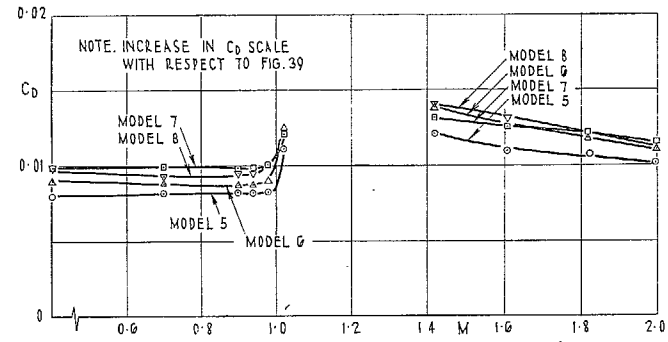
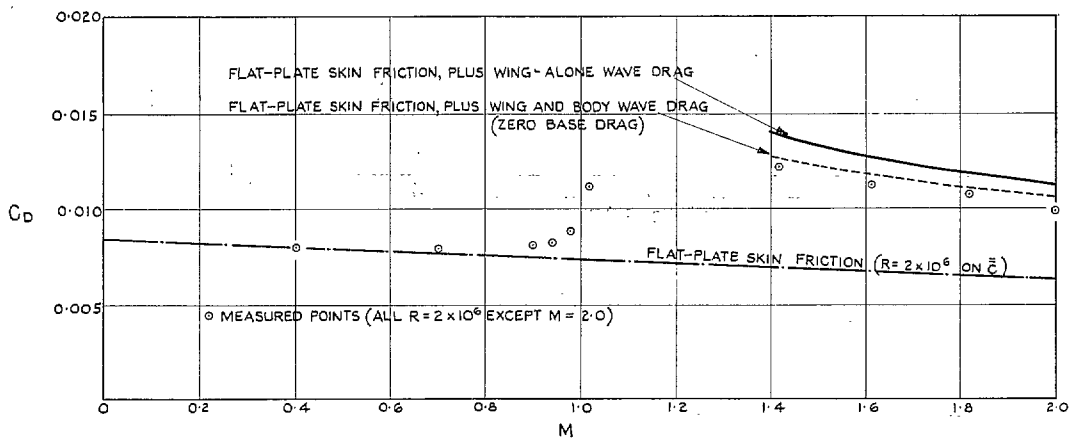FIG. 40. Variation of C_D at $C_L = 0$ with Mach number.

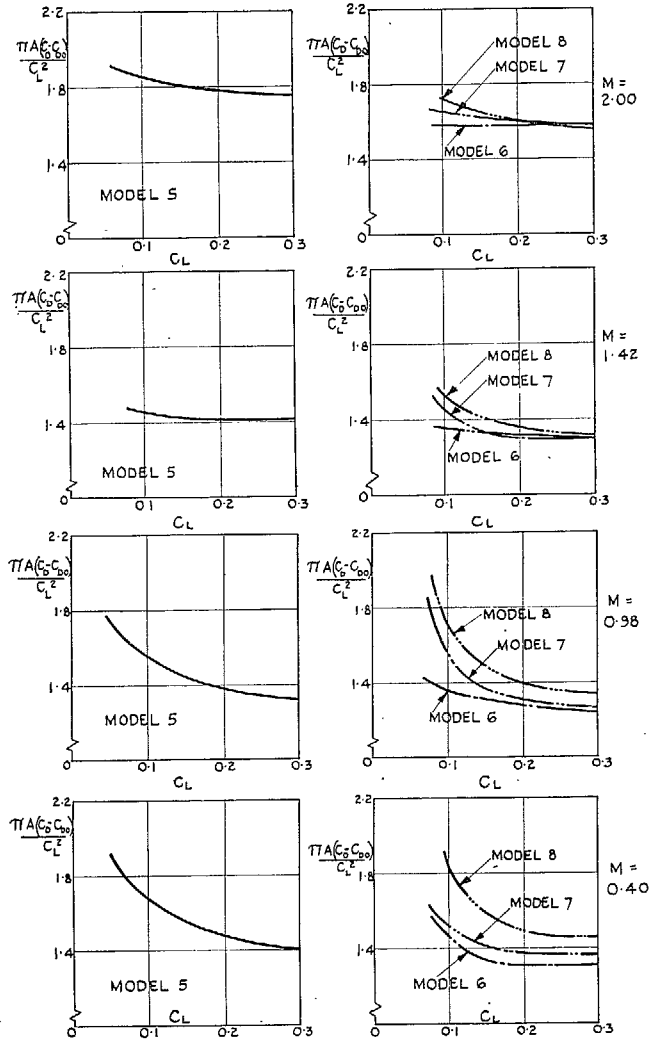FIG. 41. Comparison of zero-lift drag of uncambered wing with theory.

Fig. 42. Variation of lift-dependent drag factor
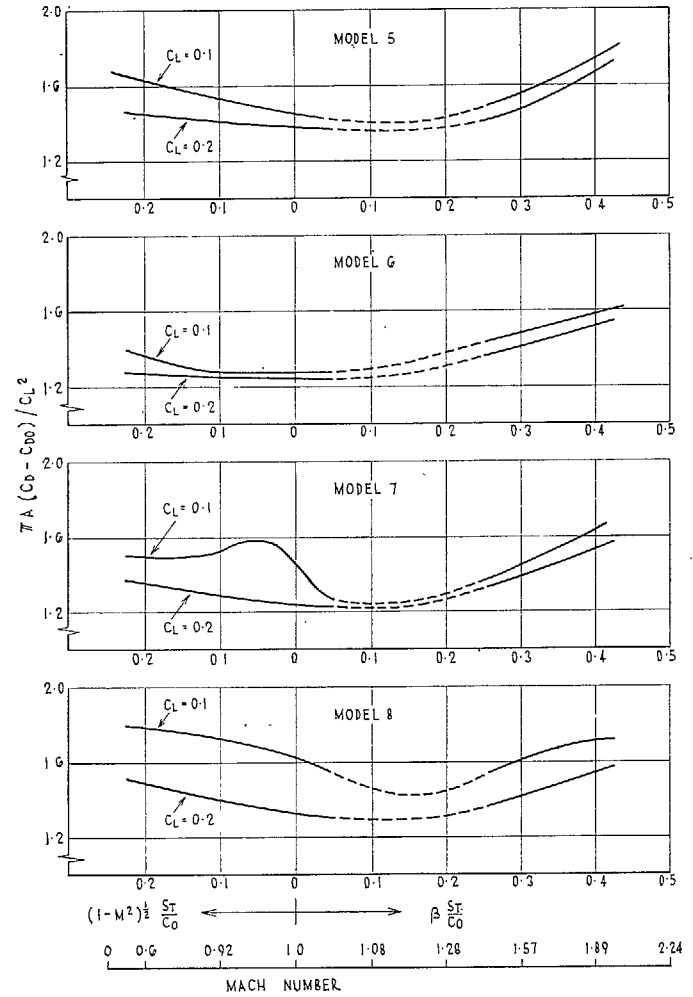with C_L and Mach number.

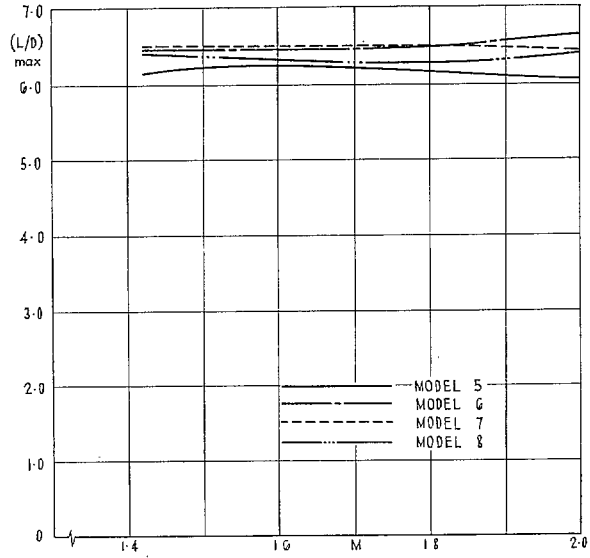Fig. 43. Variation of lift-dependent drag factor with
$\beta s_T / c_0$.

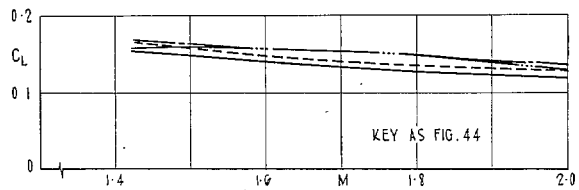FIG. 44.   Variation of $(L/D)_{max}$ with Mach
number.

FIG. 45.   Variation of C_L for $(L/D)_{max}$ with
Mach number.

47

Publications of the
Aeronautical Research Council

ANNUAL TECHNICAL REPORTS OF THE AERONAUTICAL
RESEARCH COUNCIL (BOUND VOLUMES)

1942 Vol. I. Aero and Hydrodynamics, Aerofoils, Airscrews, Engines. 75s. (post 2s. 9d.)
     Vol. II. Noise, Parachutes, Stability and Control, Structures, Vibration, Wind Tunnels. 47s. 6d. (post 2s. 3d.)

1943 Vol. I. Aerodynamics, Aerofoils, Airscrews. 80s. (post 2s. 6d.)
     Vol. II. Engines, Flutter, Materials, Parachutes, Performance, Stability and Control, Structures.
                                      90s. (post 2s. 9d.)

1944 Vol. I. Aero and Hydrodynamics, Aerofoils, Aircraft, Airscrews, Controls. 84s. (post 3s.)
     Vol. II. Flutter and Vibration, Materials, Miscellaneous, Navigation, Parachutes, Performance, Plates and
         Panels, Stability, Structures, Test Equipment, Wind Tunnels. 84s. (post 3s.)

1945 Vol. I. Aero and Hydrodynamics, Aerofoils. 130s. (post 3s. 6d.)
     Vol. II. Aircraft, Airscrews, Controls. 130s. (post 3s. 6d.)
     Vol. III. Flutter and Vibration, Instruments, Miscellaneous, Parachutes, Plates and Panels, Propulsion.
                                    130s. (post 3s. 3d.)
     Vol. IV. Stability, Structures, Wind Tunnels, Wind Tunnel Technique. 130s. (post 3s. 3d.)

1946 Vol. I. Accidents, Aerodynamics, Aerofoils and Hydrofoils. 168s. (post 3s. 9d.) ·
     Vol. II. Airscrews, Cabin Cooling, Chemical Hazards, Controls, Flames, Flutter, Helicopters, Instruments and
         Instrumentation, Interference, Jets, Miscellaneous, Parachutes. 168s. (post 3s. 3d.)
     Vol. III. Performance, Propulsion, Seaplanes, Stability, Structures, Wind Tunnels. 168s. (post 3s. 6d.)

1947 Vol. I. Aerodynamics, Aerofoils, Aircraft. 168s. (post 3s. 9d.)
     Vol. II. Airscrews and Rotors, Controls, Flutter, Materials, Miscellaneous, Parachutes, Propulsion, Seaplanes,
         Stability, Structures, Take-off and Landing. 168s. (post 3s. 9d.)

1948 Vol. I. Aerodynamics, Aerofoils, Aircraft, Airscrews, Controls, Flutter and Vibration, Helicopters, Instruments,
         Propulsion, Seaplane, Stability, Structures, Wind Tunnels. 130s. (post 3s. 3d.)
     Vol. II. Aerodynamics, Aerofoils, Aircraft, Airscrews, Controls, Flutter and Vibration, Helicopters, Instruments,
         Propulsion, Seaplane, Stability, Structures, Wind Tunnels. 110s. (post 3s. 3d.)

Special Volumes
     Vol. I. Aero and Hydrodynamics, Aerofoils, Controls, Flutter, Kites, Parachutes, Performance, Propulsion,
         Stability. 126s. (post 3s.)
     Vol. II. Aero and Hydrodynamics, Aerofoils, Airscrews, Controls, Flutter, Materials, Miscellaneous, Parachutes,
         Propulsion, Stability, Structures. 147s. (post 3s.)
     Vol. III. Aero and Hydrodynamics, Aerofoils, Airscrews, Controls, Flutter, Kites, Miscellaneous, Parachutes,
         Propulsion, Seaplanes, Stability, Structures, Test Equipment. 189s. (post 3s. 9d.)

Reviews of the Aeronautical Research Council
       1939-48   3s. (post 6d.)   1949-54   5s. (post 5d.)

Index to all Reports and Memoranda published in the Annual Technical Reports
       1909-1947   R. & M. 2600 (out of print)

Indexes to the Reports and Memoranda of the Aeronautical Research Council

Between Nos. 2351–2449	R. & M. No. 2450	2s. (post 3d.)
Between Nos. 2451–2549	R. & M. No. 2550	2s. 6d. (post 3d.)
Between Nos. 2551–2649	R. & M. No. 2650	2s. 6d. (post 3d.)
Between Nos. 2651–2749	R. & M. No. 2750	2s. 6d. (post 3d.)
Between Nos. 2751–2849	R. & M. No. 2850	2s. 6d. (post 3d.)
Between Nos. 2851–2949	R. & M. No. 2950	3s. (post 3d.)
Between Nos. 2951–3049	R. & M. No. 3050	3s. 6d. (post 3d.)
Between Nos. 3051–3149	R. & M. No. 3150	3s. 6d. (post 3d.)

HER MAJESTY'S STATIONERY OFFICE
from the addresses overleaf